ABSTRACT

Title of Document:	A SELF-CONTAINED COLD PLATE UTILIZING FORCE-FED EVAPORATION FOR COOLING OF HIGH-FLUX ELECTRONICS
	Thomas Buchanan Baummer, Master of Science 2007
Directed By:	Professor Michael Ohadi, Mechanical Engineering

In recent years, the rapid increase in the functionality, speed, and power density of electronics has introduced new challenges, which have led to demand for high heat flux electronics cooling at levels that cannot be met by conventional technologies. The next generation of high power electronics will require advanced cooling beyond the methodologies currently available. This thesis describes work done on a novel form of two-phase heat transfer, named "Force-Fed Evaporation," which addresses this need. This process utilizes evaporation of a liquid in a microchannel surface to produce high heat transfer coefficient cooling at very high heat flux while maintaining a low hydraulic pressure drop. Component level tests were conducted to demonstrate the capability of this process. This led to the development of a self-contained, two-phase cold plate suitable for cooling a high power circuit board. The results show that this technology bears promise for the future of electronics cooling.

A SELF-CONTAINED COLD PLATE UTILIZING FORCE-FED EVAPORATION FOR COOLING OF HIGH-FLUX ELECTRONICS

By

Thomas Buchanan Baummer

Thesis submitted to the Faculty of the Graduate School of the
University of Maryland, College Park, in partial fulfillment
of the requirements for the degree of
Master of Science
2007

Advisory Committee:
Professor Michael Ohadi, Chair
Professor Reinhard Radermacher
Professor Bao Yang

Dedication

This work is dedicated to my wife, Lisa, and to my parents, whose encouragement helped me to complete it and who have supported me always.

Acknowledgements

I would like to thank Dr. Serguei Dessiatoun for all of his help in conducting this research. What I learned from him I will always carry with me. I would also like to thank my advisor Dr. Michael Ohadi and Dr. Amir Shooshtari for their support and guidance on this project. I also owe a debt of gratitude to Edvin Cetegen who worked with me on parts of this project, and especially to Mark Specter and the Office of Naval Research who provided the financial support that made this research possible.

Table of Contents

List of Tables

List of Figures

Chapter 1: Introduction

1.1: Electronics Cooling Needs and Methods

Since the invention of the abacus in ancient times, people have been using tools to help them perform mathematical problems. Such simple tools were replaced by mechanical calculators, which were in turn replaced by the earliest computers. In the mid 20th century, these were replaced by the digital computers in use today. Along the way, the problems being solved with these tools have gone from basic arithmetic to complex simulations of three-dimensional processes including mass, momentum, and energy balances. To solve these kinds of problems, computing power has increased by dramatic leaps during the past few decades; Moore's Law states that computing power doubles every 18 months. This increase in computing power has been achieved by creating transistors that are faster and smaller—allowing them to be packed ever more densely into integrated circuits. However, both of these changes come at the price of making computers ever more power hungry.

Modern integrated circuits consist of millions of transistors acting to control the flow of electrons. These are built up into logic circuits, which are built up into advanced processing devices. As they operate, all of the energy they use or waste is eventually converted to heat, which must be dissipated to the surroundings. The more transistors a device contains, the more heat that needs to be removed from it. It is now common for a PC to have a power supply capable of delivering

300-400 watts or more, and high power applications can consume vastly more power than this. As the size of the chips generating this heat continually shrinks, the heat flux that needs to be dissipated has been increasing significantly and will continue to do so. It is projected that the heat dissipation needs for specialized applications will reach 100 W/cm^2 (1,000 kW/m^2) in the near future. In order for an integrated circuit to operate properly, it must be kept relatively cool—typically below 70°C for commercial applications or 125°C for the military [1]. It is these temperature restrictions that dictate the use of advanced cooling technologies for high power applications.

For low-power computer chips, it is sufficient to cool the device via natural convection in air—simply leave enough open space near the chip and the hot air rising from the device will draw up cooler air at a rate fast enough to remove all of the heat. For higher power circuits—which now includes many of the basic components of a PC—natural convection cannot remove heat fast enough to keep the temperature of the electronics sufficiently low. For these applications, an improved level of heat removal is obtained by utilizing a fan for forced convection of air across a finned heat sink [2]. However, for advanced computer applications—including supercomputers, some servers, and various military applications—fan cooling is also unable to remove all of the heat generated. In such cases, the next level in increased heat removal capability is reached though the use of either liquid cooling or two-phase cooling.

Liquid cooling generally consists of forced convection of some working fluid over a flat plate or—more commonly—through some finned heat sink [3]. A major difference between liquid cooling and air cooling is that liquid cooling systems are generally closed systems. When a device is air-cooled, it is rejecting heat to a nearly infinite medium; cool air is always available to feed to the device as warm air is rejected away from the system. With a liquid-cooled device, the liquid is recirculated within the system because there is no semi-infinite liquid medium to which heat may be rejected. Thus, liquid-cooled systems must include a second heat exchanger to remove heat from the liquid—generally by rejecting that heat to the air. So for both air-cooled and liquid-cooled systems, the final destination of the thermal energy is the surrounding air; the advantage of liquid-cooled systems is that they can remove heat at a high heat flux at the computer chip and then dissipate it to air over a considerably larger area. Liquid cooled systems for PC's can reach or exceed 200 W/cm^2 of heat dissipation, and more advanced cooling systems have been developed for more advanced electronic applications [3].

The most advanced electronic cooling technologies are those that take advantage of a fluid's latent heat of vaporization by incorporating phase change from liquid to vapor. Like liquid-cooled systems, these two-phase systems must operate in a continuous cycle that rejects heat to its environment (the air). The heat is absorbed from the electronics at the evaporator and rejected to the environment when the vapor condenses in the condenser. The simplest two-phase cooling

technologies are heat pipes and thermosyphons. These are both passive technologies that incorporate fluid in a sealed tube that boils at the evaporator surface, moves to a condenser, and then returns to the evaporator [2]. A thermosyphon relies on gravity to transfer the liquid to the evaporator surface. The condenser is positioned above the evaporator, so that condensate is drawn to the evaporator by gravity. A heat pipe is a similar device, which uses a wicking structure to draw liquid from the condenser to the evaporator. This allows the system to work regardless of its orientation, which is advantageous for cooling physically complicated systems.

A more complicated—but also more effective—two-phase cooling mechanism is spray cooling. With this method, pressurized liquid is forced through a nozzle to spray onto the electronics' surface [4]. The droplets vaporize quickly on the hot surface due to their small size, and the vapor produced effectively carries away the heat. With this method, the flow rate is controlled by a pump, which allows high flow rates to be selected for improved performance. However, this method requires a significant amount of pumping power, and the fluid used must be dielectric to prevent damaging the electronics being cooled.

It is expected that the cooling needs of advanced electronics will soon exceed the capabilities of the cooling methods currently available. For this reason, much research—which is discussed in the next chapter—has been focused on developing more advanced systems for electronics cooling. Such systems are also

likely to be applied to a variety of other applications once they are commercialized. The present research seeks to develop an advanced method for electronics cooling, which will meet the ever increasing demand for electronics heat removal and will outperform both the currently established cooling mechanisms as well as those new ones currently being developed.

1.2: Motivation and Objectives

The above section explained why new methods of electronics cooling will be needed in the near future. This project was conceived to investigate the performance of a novel cooling method and develop that method into a functional electronics cooling system capable of cooling large electronics circuit boards for a variety of applications. This new cooling method is called Force-Fed Evaporation or Force-Fed Condensation and is described in detail in Section 3.1. It is believed that this technology has the capability to outperform spray cooling and other advanced cooling technologies in terms of its thermal performance. More importantly, force-fed technology can significantly outperform most other single-phase and two-phase technologies in terms of the pressure drop through the device, which directly corresponds to the pumping power consumed by the cooling system.

This research has two principal objectives, which were alluded to in the above paragraph. This work will investigate the performance of the force-fed evaporation process and it will demonstrate the applicability of this technology to

cooling electronics by developing a complete two-phase cooling device. The first objective will be met by a series of component-level tests that focus on the ability of a single force-fed evaporator to remove heat from a heated surface and dissipate it to a two-phase working fluid. Because these tests focus solely on evaporator performance, the other system components—condenser, pump, reservoir, and instrumentation—can be as large or complicated as is reasonable to fulfill their support role to the evaporator. The second objective is met by developing a complete, two-phase cooling system, which is self-contained within a cold plate. All of the system components will be designed and sized to fit in a cold plate that is roughly equal in size to the electronics board it cools. The tests of this cold plate will focus on its ability to remove a given amount of heat from multiple heat sources and dissipate is via condensers to an external water supply. Meeting the second objective demonstrates that this technology is a viable, marketable method for cooling electronics and may be capable of displacing existing and future cooling technologies.

These two objectives are closely linked, because the results of the first, component-level tests will be used to develop the design and expectations for the system-level device. The organization of this report treats the two objectives as parallel paths. Thus Chapter 3 describes the design of the component-level tests, Chapter 4 describes the design of the system-level tests, then Chapter 5 provides the component-level results, and Chapter 6 provides the system-level results. Finally, with all of the results of these tests presented, Chapter 7 discusses

conclusions and recommendations for future research regarding this force-fed technology.

Chapter 2: Literature Review

As described in the first chapter, there is a great need for advanced cooling methods for high power electronics. Since the early 1980s, hundreds of research articles have reported investigations on the mechanics, performance, and applications of microchannel cooling. Most of this research was begun by Tuckerman and Pease [5], who first proposed the use of microchannels to cool very large-scale integrated circuits (VLSI's). In the years since, researchers have studied microchannel flows from every imaginable perspective, from fundamental investigations in single tubes, to visualization studies, to application-based tests of hybrid cooling devices. This chapter provides an overview of the kind of work that has been done in this field and is relevant to the present work. Specifically, the focus is on boiling flows in microchannel heat sinks. Jet impingement in microchannel heat sinks is also covered because of the parallels that exist between jet impingement and the present work.

2.1: Microchannel and Minichannel Studies

Kandlikar has produced a summary of the mechanisms at work in microchannel evaporation [6], which serves as a good introduction to the research that has been done in this field. The governing forces he identifies for evaporating flows in microchannels are surface tension, viscous shear forces, inertial forces, and the momentum change caused by the evaporation of the liquid. The small channel sizes lead to very low Reynolds numbers, which implies that nucleate boiling will

be the dominant mode of heat transfer—something that is confirmed by most experimental research. The small channel size also reduces the number of suitable nucleation sites, which increases the wall superheat necessary to initiate boiling compared with conventional sized channels. Because of this, when boiling does begin, it frequently progresses very rapidly, often filling the entire channel with vapor. This sudden evaporation in a microchannel can lead to unstable flow, including reversed flow, which is especially common in heat sinks containing numerous parallel microchannels.

Kandlikar also discusses the heat transfer mechanisms that occur during microchannel evaporation. After nucleate boiling begins, a vapor plug travels down the channel. At the leading edge, contact line evaporation exists on the whole perimeter of the channel. Around the plug, thin film evaporation occurs until dryout occurs on the channel walls. As part of this review, Kandlikar proposes a set of criteria for classification of channel size, which, although arbitrary, has been used by many other researchers in the absence of physics-based criteria. Channels with a hydraulic diameter greater than 3 mm are considered conventional channels. Minichannels have hydraulic diameters from 200 μm to 3 mm, and microchannels fall between a hydraulic diameter of 10 and 200 μm.

The most fundamental research in small channel boiling is the study of boiling in a single tube or channel in great detail. This has a direct application to

conventional heat exchangers, so most of the work in this realm is done with refrigerants and uses channels in the minichannel size range. One such study was conducted by Boye et al. [7]. They tested a 1.5 mm diameter, 500 mm long tube oriented vertically with boiling water flowing upwards. They ran their test setup for mass fluxes from 50 to 100 kg/m^2-s and heat fluxes from 10-115 kW/m^2 and for conditions of single-phase, subcooled boiling, and saturated boiling. In their two-phase tests, they observed that the heat transfer coefficient increased in the single-phase region to a local maximum at the onset of nucleate boiling. The heat transfer coefficient then decreases, but rises again to its global maximum value in the convective boiling regime. They observed heat transfer coefficients up to 18 kW/m^2-K at 94.7 kW/m^2 heat flux and 50 kg/m^2-s mass flux. They concluded that convective boiling dominates at high heat fluxes.

A similar study was conducted by Pamitran et al. [8]. They studied the boiling of R-410A in horizontal stainless steel tubes with diameters of 1.5 and 3 mm and lengths of 1.5 m and 3 m, respectively. They applied heat fluxes of 10-30 kW/m^2 and mass fluxes of 300-600 kg/m^2-s. They observed that changing the mass flux has no effect on the heat transfer coefficient at low qualities, which they interpreted as showing that the heat transfer in this region was dominated by nucleate boiling. At higher qualities, where the annular flow regime occurs, nucleate boiling is suppressed in favor of convective boiling, and they observed that increases in the flow rate increased the heat transfer coefficient. They also observed a spike in the heat transfer coefficient just before dryout occurred due to

the annular liquid layer becoming very thin. For 20 kW/m^2 and a mass flux of 600 kg/m^2, they detected a maximum heat transfer coefficient of 20 kW/m^2-K at a quality of 0.55.

Another study done on single minichannels was conducted by Bao et al. [9]. They studied evaporation of R-11 and HCFC-123 in a 1.95 mm diameter copper tube 870 mm long with a 200 mm active test section near of the middle of the length. Their experiments covered a wider range of heat and mass fluxes: 5-200 kW/m^2 and 50-1,800 kg/m^2-s. Their study also included qualities from 0 to 0.9 and inlet pressures of 200-500 kPa. They observed heat transfer coefficients from 1 to 18 kW/m^2-K. From their results, they found that the heat transfer coefficient is a strong function of heat flux and pressure, but that mass flux and vapor quality only showed a small effect within their experimental range. From this information, they concluded that nucleate boiling was the dominant mode of heat transfer in their channel, and that convective effects were minimized by the low Reynolds number and low liquid conductivity. Like Boye et al., Bao et al. also found that the heat transfer coefficient increases up to the point of onset of nucleate boiling; however, they found it to be independent of quality thereafter. They also found that the two refrigerants produced very similar heat transfer. For one test using HCFC-123 at 125 kW/m^2 and 452 kg/m^2-s, the maximum heat transfer coefficient observed was about 14 kW/m^2-K.

Diaz and Schmidt undertook an investigation of the unsteady effects of boiling in a single minichannel [10]. Unlike the studies above, their channel was a 0.3 mm by 12.7 mm rectangle and was 200 mm long. Both water and ethanol were used as working fluids with mass fluxes of 50 to 500 kg/m^2-s. The applied heat flux was up to 400 W/cm^2 (40 kW/m^2). They first tested the single-phase pressure drop in their channel and found it to be in good agreement with existing correlations. To quantify the unsteadiness of the flow, they measured the oscillations in the wall temperature using infrared thermography. With water, they found that temperature oscillations increased with increasing heat flux and decreasing mass flux. A typical oscillation was in the range of 20°C. The largest oscillations were before the onset of nucleate boiling, after which point the oscillations decreased in magnitude. For ethanol, the magnitude of the oscillations was much smaller across the board—on the order of a few degrees. However, with ethanol, the oscillations increased slightly to about 5°C with increasing quality after the onset of boiling. For water, the heat transfer coefficient peaked at the onset of nucleate boiling and then decreased with increasing quality. Ethanol behaved similarly, with a relatively lower peak except at low heat fluxes, where after peaking at the onset of nucleate boiling, the heat transfer coefficient gradually increased again at higher qualities. Heat transfer coefficients of 160 kW/m^2-K for water and 65 kW/m2-K for ethanol were observed at a mass flux of 500 kg/m^2-s.

A number of authors have undertaken studies of complete microchannel heat sinks. These devices are especially applicable to cooling of high power microelectronics. The numerous parallel channels in these devices typically have hydraulic diameters within the microchannel range, and the interactions between these channels open up a whole new set of variables to be investigated. One study in this area was conducted by Jiang et al. [11]. They developed a microchannel array made by cutting into a silicon wafer and then covering it with glass to form complete channels. They tested two versions of their device. Each was 10 by 20 mm with 18.6 mm long channels; one device had 35 50 μm wide channel (26 μm in hydraulic diameter), the other had 34 100 μm wide channels (53 μm in diameter). A heater and a temperature sensing array sat beneath the silicon channel base. They observed nucleate boiling for both diameter channels at low heat flux; at higher heat fluxes they observed annular flow in both. They found that when the temperature difference and heat flux were normalized using the temperature and heat flux at the critical heat flux (CHF), all of their data fell on approximately the same curve. For q"/CHF < 0.4 they saw no boiling. From a normalized heat flux of 0.4 to 0.6, they observed bubbles forming in the inlet and outlet regions of the heat sink, which were then forced through the microchannels at high speed. From 0.6 to 0.9, they observed stable annular flow. Typical values for their setup were a flow rate of 2 ml/min (~1,794 kg/m^2-s) and a CHF of 29.9 W (~1.5 kW/m^2).

A similar study of a microchannel heat sink was conducted by Chen and Garmimella [12]. Their heat sink consisted of a 25.4 by 25.4 by 7 mm copper block with 10 channels cut into it, each one 504 μm wide and 2.5 mm deep for an aspect ratio of 5 and a hydraulic diameter of 839 μm. The Flourinet fluid FC-77, manufactured by 3M (St. Paul, MN), was used in their tests. They measured the heat transfer coefficient as well as the critical heat flux in their experiments and found that both rise with increasing flow rate. They also noted that at higher flow rates, the heat transfer rate near CHF approaches the limiting rate of evaporation, from which they concluded that convective heat transfer is less important at high heat fluxes. During their experiments, they observed bubbly flow with oscillations, including flow reversal, in their test section. They measured heat transfer coefficients up to 6 kW/m^2-K and CHF from 13 W/cm^2 at 30 ml/min to 21 W/cm^2 at 50 ml/min. In comparing their data to a number of boiling correlations, they found that Cooper's nucleate boiling correlation matched their measured data very well. Another notable finding of theirs was the observation that the heat transfer coefficient was slightly higher for low flow rate at lower wall temperatures, but at higher wall temperatures, the higher flow rate generated a higher heat transfer coefficient.

A third experimental study of heat transfer in a minichannel array was conducted by Yun et al. [13]. Their study differs from the previous two in that their test section consisted of extruded aluminum minichannels, rather than discrete channels cut into the top of a block. The hydraulic diameters were 1.44 mm and

1.36 mm for the two arrays they studied. They tested this heat sink using R-410A for heat fluxes of 10-20 kW/m^2 and mass fluxes of 100-400 kg/m^2-s. They observed that changing the saturation pressure had no effect the heat transfer coefficient before the point of "dryout vapor quality" (around 0.55), but that after this point, higher pressures led to increased performance. They attributed this effect to the fact that the liquid and vapor densities are closer at higher pressures, which improves flow distribution. Similar to what other authors have found, Yun and his colleagues observed that prior to dryout quality, heat flux, mass flux, and pressure have no effect on the heat transfer coefficient, but after that point, heat transfer increases with an increase in any of these three parameters. They attained heat transfer coefficients up to about 20 kW/m^2-K for the 1.36 mm diameter channels with a heat flux of 15 kW/m^2 and a mass flux of 300 kg/m^2-s. This was twice as high as the performance of a single tube tested under similar conditions. As with circular tubes, they found that pressure drop increased with increasing flow rate, and decreased with increasing temperature; however, the minichannels had a higher pressure drop for the same temperature and mass flux due to their larger perimeter for the same flow area. Pressure drops for their tests fell between 7 and 40 kPa per meter.

Some studies of boiling in microchannel heat sinks have taken a narrower focus. Rather than investigating all aspects of the situation, certain parameters or aspects of such arrangements are studied in detail. One area of interest is the stability criteria for boiling in microchannel arrays. As mentioned by Kandlikar above [6],

the rapid evaporation in channels and the interaction between channels can lead to flow instabilities. Jiang et al. [11] observed this with the formation of vapor bubbles in the inlet manifold—a situation made possible by the high superheat required for boiling in the channel itself. Chen and Garimella [12] observed instabilities in the form of oscillating and revered flow in their test section.

One study that investigated microchannel array stability in detail was conducted by Chang and Pan [14]. Their heat sink consists of 15 parallel microchannels with hydraulic diameters of 86.3 μm; they used a high-speed camera to observe the flow patterns. They used water with flow rates from 0.01 to 10 ml/min (about 1.9 to 1,900 kg/m^2-s). At 22 kg/m^2-s and 7.91 kW/m^2—the point of onset of nucleate boiling—they observed the following progression of flow patterns: a single bubble would nucleate in a channel then grow into a vapor slug and lengthen; at the flow exit, slug or annular flow would exist. They observed that the pressure field around the bubbles suppressed growth of any other bubbles, and that variations in the pressure field made bubble growth erratic. At the same mass flux, but twice the heat flux, they observed unstable boiling, including flow reversal, with both slug and annular flow. They also noted that large fluctuations in the pressure could cause bubbles to alternately grow and shrink. In trying to classify the stability of microchannel arrays, the authors noted that pressure drop fluctuations greater than about 6 kPa (compared to an average pressure drop that ranged from 5 to 35 kPa for their tests) were indicative of significant instabilities in the system. In comparing their results with a flow regime map, they concluded

that there was only a small range of subcooling numbers and phase change numbers where the flow could be stable; this was found to be near the line representing zero outlet quality.

Another detailed study on a minichannel array was conducted by Kandlikar and Balasubramanian [15]. They studied the effect of gravitational orientation on small channel evaporation. Because the viscous and surface tension effects are large at a smaller scale, it was expected that the effect of gravity would be small. Their test setup consisted of 6 parallel channels 1054 μm by 197 μm (hydraulic diameter of 333 μm) and 63.5 mm long. Water was sent through the channels horizontally, vertically upward, and vertically downward at a flow rate of 120 kg/m^2-s with a heat flux of 317 kW/m^2 and an outlet quality of 0.38. As other researchers have found, they observed plug flow in their channels; however, they also noted nucleate boiling in the thin film around the vapor plug where others have observed only convective boiling. Like Chang and Pan, Kandlikar and Balasubramanian observed bubbles being shrunken by the growth of neighboring bubbles, and even observed those bubbles to occasionally disappear altogether. In downward flow, churn flow was caused by the breakup of vapor plugs. In all cases, backflow was present; however, it was most significant in downward flow where bubbles would reach the inlet manifold and damage the flow distribution between channels. In general, they found that upward vertical flow was less chaotic, while downward flow exhibited the most flow reversal.

In addition to experimental studies like those mentioned above, a number of researchers have used numerical or analytical models to further the understanding of microchannel flow. This approach has the advantage that, using commercial fluid dynamics software, it is often possible to design and run an experiment much faster than can be done physically. The disadvantage is that the physics of the situation must be well understood in order to be programmed into the software, and the microchannel effects are not fully understood or identified. Additionally, it is difficult or impossible to model phase changing flow without significant simplifications. Nonetheless, numerical models are useful tools, particularly for running parametric studies for determining how variations of a given parameter affect a system.

Chen [16] developed an analytical model for single-phase flow in microchannels that were represented as a porous medium. His model was unique in that he included the effects of inertia, which are sometimes excluded by reason of the small channel size. He observed that the Nusselt number increased with increasing porosity and aspect ratio. From an aspect ratio of 1 to about 3.5, this increase was very significant; from 3.5 to 10, the increase became more gradual. He also found that including inertia in the model decreased the velocity significantly, particularly at higher aspect ratios. Decreasing the effective ratio of liquid to solid conductivity also increased the Nusselt number because this allowed more heat to be conducted to higher points in the channels.

Another numerical and analytical analysis was conducted by Zhao and Lu [17]. They compared the results obtained through 2-D analysis using the porous medium approach and the fin approach for single-phase flow through a microchannel heat sink. Using the fin method, the fluid is assumed to have no temperature variation in the direction perpendicular to the flow. Like Chen, they found that the Nusselt number was increased by increasing the aspect ratio or decreasing the liquid-solid conductivity ratio. However, they found that the fin method gives too little variation in the temperature of the solid compared with the porous medium approach, which has been shown by other researchers to be accurate to within about 4%. Additionally, the fin approach overestimates the heat transfer by about 2 times. With the fin approach, no optimum porosity was identified, but with the porous medium approach an optimum porosity was identified, which varied almost linearly from 0.9 at an aspect ratio of 1 to 0.5 at an aspect ratio of 10. The authors also modeled the effect of building micro heat pipes into the heat sink. These were modeled as small vertical tubes with conductivity 10 times greater than copper, which would help conduct heat up the height of the channel walls. For high conductivity fluids, the heat pipes approximately doubled the Nusselt number at an aspect ratio of 10. As one might expect, the effect was less significant for smaller aspect ratios.

As mentioned at the start of this chapter, this review is intended not as a comprehensive assessment of all studies in the field of microchannel boiling. Rather, it is a brief introduction to the multitude of investigations done in this

field. For a more complete description of the work in this field, a number of review papers have been published and are available. Kandlikar [18] has published a review of flow patterns, pressure drop, and heat transfer for boiling in small channels in which he draws conclusions and identifies similarities from across the body of literature. He notes that because of the large effect of surface tension, stratified flow is rarely seen, while slug and churn flow are found over a wide range of parameters. Only at mass fluxes less than 21 kg/m^2-s is stratified flow sometimes observed. The heat transfer coefficient is found to generally depend on the flow regime. In the isolated bubble region, it is proportional to the applied heat flux. In the confined bubble region, there is less dependence of heat transfer on heat flux, and in the annular-slug region, convective effects dominate the heat transfer. A number of authors observed nucleate boiling within the thin film surrounding the vapor slug, as did Kandlikar and Balasubramanian in the study described above [15], and these generally did not quickly join with the main vapor bubble. He also found that for low Reynolds numbers, where the shear stress is low, the bubble growth rate was comparable to pool boiling growth rate, whereas in turbulent flow, the bubbles grew much more quickly. Finally, he observed that flow instabilities could be reduced by increasing the pressure drop in the region upstream from the microchannel array. In many experimental setups, it was the low pressure drop inlet manifold that allowed the flow to reverse.

Two literature reviews by Thome provide more insight into the breadth of information on this subject [19,20]. He notes that the dominant flow regimes seen in studies are elongated bubble and annular flow. In the literature, he finds that the heat transfer coefficient depends mostly on heat flux and saturation pressure, which leads to the conclusion that nucleate boiling is the dominant heat transfer mechanism. However, Thome presents a model that uses thin film evaporation as the dominant mechanism and thus shows an effect of mass velocity and vapor quality on the heat transfer coefficient. Among experimental studies, he lists a number of criteria which should be present for a completely valid experiment but which were not entirely present in any of the studies. These criteria include running the test section with laminar and turbulent single-phase flow to test it against known correlations; reporting surface roughness, which should play a role in nucleate boiling; comparing results with other researchers for the same fluid, channel diameter, and conditions; reporting day-to-day repeatability of the results; confirming that steady state had been reached, which is difficult to determine due to the instability in the flow; reporting subcooled as well as saturated inlet conditions; and including enthalpy change with pressure in determination of quality.

Thome also finds existing conventional-scale correlations to be inadequate for microchannel boiling because they assume turbulent flow and nucleate boiling as the primary method of heat transfer [19]. Instead, he presents his own two-zone model consisting of heat transfer to liquid slugs and long bubbles. The heat

transfer to the liquid is relatively insignificant and is ignored, while thin film evaporation is used for heat transfer in the region of the bubble. He claims that this model is the best match to existing experiments and that experiments that showed no effect of mass velocity or quality were conducted under conditions where variation of these parameters would have a small effect.

In the second review, Thome focuses on research areas that should be pursued to develop microchannels as a viable technology for cooling electronics [20]. His list of focus areas includes predicting CHF, understanding void fraction, developing a functioning flow pattern map, optimizing the two-phase pressure drop, calculating and measuring local heat transfer coefficient, and finding a lower limit for flow rate based on instabilities. Other things that he says should be taken into account are the best fluids for various applications, fin and channel shape effects, and the transient conditions that would be induced at start-up. Regarding the flow pattern map, he lists the following flow regimes that have been reported in the literature: bubbly, bubbly/slug, slug, slug/semi-annular, semi-annular, wavy annular, and smooth annular. In addition, some researchers have proposed a liquid ring flow that resembles annular flow with a short region where the film is thicker, forming a ring. Others have proposed an explosive flow at high heat fluxes where rapid bubble growth forces liquid out of the channel in both directions, and a wedging flow regime where part of the perimeter of a vapor slug dries out as the bubbles pass. The trends Thome observes for heat transfer coefficient partially agree with what has been presented above: that below a

quality of 0.5, heat transfer increases with heat flux and decreases slightly with quality, and that after this point the heat transfer increases significantly with quality but is independent of heat and mass flux.

2.2: Jet Impingement Studies

The second part of this literature review is devoted to covering a few of the many works done in the field of jet impingement. As mentioned at the start of this chapter, there are parallels between jet impingement into a microchannel heat sink and the processes developed in the present work. Zhuang et al. [21] studied the performance of a slot jet directed at a rectangular target where the distance from the target to the jet plate was close enough for the device to operate as a two-dimensional microchannel. The slot was 12 mm long and 146, 210, or 234 μm wide, depending on the test. The distance between the nozzle and the target varied from 0.1 to 0.58 mm, creating a confined jet. The fluids used were transformer oil, with Reynolds numbers from 70 to 170, and the 3M fluid FC-72, with Reynolds numbers from 911 to 4807. They studied the effects of velocity, channel size, and Prandtl number on the heat transfer. For both fluids they observed Nusselt numbers up to about 200. They also saw a heat transfer coefficient increase over flow between flat plates of 40-120% for oil and 75-225% for FC-72 which they attributed to the effects of the turbulence generated by the jet.

Jang et al. [22] conducted an experimental and numerical investigation of the heat transfer of an impinging jet into a microchannel heat sink and compared the results with numerical results for parallel flow in a microchannel heat sink. They developed this heat transfer method because they believe the pressure drop in parallel flow through microchannels is too high, while manifold microchannels are too bulky. Their heat sink consisted of a 10 by 10 mm base with minichannels 200 μm wide and 1400 μm tall, separated by fins 200 μm wide. Using air as their working fluid, their flow rates of 10-60 liters per minutes (approximately 24 to 143 kg/m^2-s) required pumping powers of 0.011 to 1.313 W. At 60 liters per minute, their minimum thermal resistance was 4 °C/W, which corresponds to a heat transfer coefficient of approximately 2.5 kW/m^2-K. At a fixed pumping power, their jet impingement arrangement outperformed the parallel microchannels by 48.5%. By comparison, they reported that a manifold channel arrangement outperformed parallel microchannels by only 35%.

In a later study, Jang and Kim present more work done with the same setup, with more detailed reporting of the pressure drops [23]. With a channel width of 600 μm and a flow rate of 60 liters per minute, the pressure drop was 2.5 kPa for a 600 μm channel height and 1 kPa for 1400 μm channel height. With a channel width of 800 μm, the pressure drops were 1 kPa and 650 Pa for heights of 1400 and 2200 μm, respectively.

Lee and Vafai [24] conducted a comparison between jet impingement and microchannel cooling to determine which was more suitable for cooling applications. For jet impingement, they considered submerged jets because these give the best heat transfer. They noted that in an array of jets, they must be close enough to avoid interfering with one another before reaching the target surface, and that exhausting the spent flow from one jet can decrease heat transfer at downstream jets except for very small target-nozzle distances. For microchannels, they noted that increasing the aspect ratio increases the flow rate for the same allowed pressure drop. For the comparison between jet impingement and microchannels, they simulated analytically the flow of water at 50°C with an aluminum target/heat sink. The pressure drop allowed was 200 kPa, and the heat flux up to 400 W/cm^2. They found that microchannels are the better choice for surfaces smaller than about 7 cm by 7 cm. For larger surfaces, the pressure drop in the channels required a low flow rate, which hurt the heat transfer performance and made jet impingement the better choice.

2.3: Advanced Heat Sink Designs

The final part of this literature review is devoted two novel heat sink designs which cannot neatly be classified as jet impingement or traditional flow through microchannels. These two studies serve as an excellent introduction to the rest of this work, which follows their example of creating innovative uses for microstructures to improve heat transfer. The first study is a numerical analysis of a manifold microchannel heat sink proposed by Copeland et al. [25]. This is

the same manifold heat sink referenced above by Jang et al. [22]. This device consists of a microchannel heat sink with a manifold placed on top of it to direct fluid into the microchannels without requiring it to travel the whole length of the microchannel. A schematic of this device is shown in Figure 1 below.

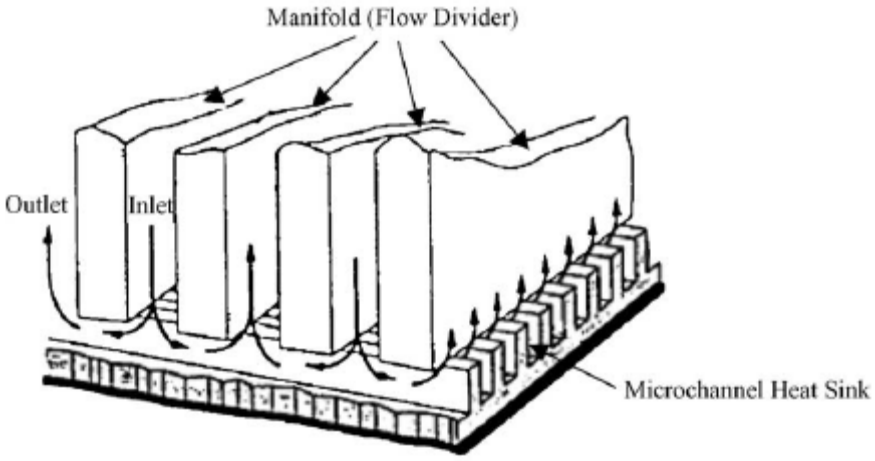

Figure 1: Schematic of Manifold Microchannel Heat Sink. Adopted from [26]

The authors recommended this heat sink in place of a traditional microchannel heat sink for cooling of electronics because it would even out the temperature distribution, allow heat sinks to be placed more densely without need for inlet and outlet manifolds beside the devices, and limit the shear stress on the device attachment because fluid travels equally in both directions. Additionally, they recommended that the manifold be held in place by compression so that thermal expansion of the manifold does not stress the device below.

For their analysis they treated the heat sink as silicon and used a fluorocarbon liquid for cooling. The dimensions of their device varied from a minimum of 400 μm manifold pitch, 150 μm channel depth, and 56.6 μm channel width to a

maximum of 1000 μm manifold pitch, 200 μm channel depth, and 113.4 μm channel width. The inlet velocity was varied from 0.1 to 1 m/s. Their analysis assumed that the walls of the channels were at a uniform temperature. They found that the maximum heat transfer coefficient occurred near the inlet, and that at higher velocities, a secondary maximum existed at the channel base below the inlet and at the top of the channel near the exit. Their reported thermal resistance at an inlet velocity of 0.1 m/s varied from 1.85 ℃/W at dimensions of 400 μm , 150 μm, and 56.6 μm to a minimum of 0.91 at 1000 μm , 200 μm, and 28.3 μm. The pressure drops for these two cases were 59 Pa and 280 Pa, respectively. At this velocity, the manifold pitch had little effect on thermal performance. Narrower channels improved performance the most, while taller channels generated some additional improvement.

The second advanced heat sink to be covered was developed and studied by Sung and Mudawar [27]. They created a hybrid jet impingement-minichannel cooling device, which is shown in Figure 2. The device consists of an array of five minichannels which have fluid supplied by means of rectangular jets in the top center of each channel. The channel width, depth, and length were 1.59 mm, 1.02 mm, and 20 mm, respectively, and the jet width and length were 0.49mm by 12.7 mm.

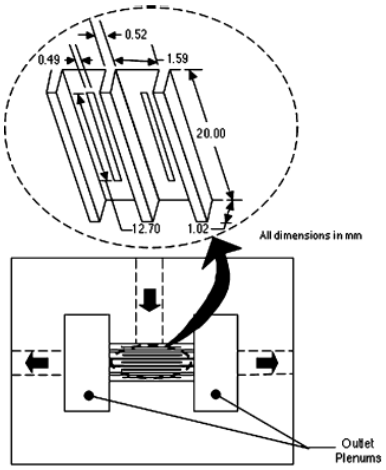

Figure 2: Diagram of Hybrid Jet Impingement and Microchannel Flow Test Section. Adopted from [27]

Using this setup, they measured the critical heat flux and device temperature for two-phase flow of PF-5052, a Flourinet fluid. In their experiments, they varied flow rate from about 1.5×10^{-5} m^3/s to about 6×10^{-5} m^3/s and subcooling from 13℃ to 34℃. These flow rates correspond to approximately 482 kg/m^2-s and 1,928 kg/m^2-s at the slot entrance. For each set of conditions, the heat flux was gradually increased until CHF was reached. They obtained CHF values of 100-200 W/cm^2 and found that increased flow rate and increased subcooling both increased CHF, though flow rate had a more significant effect over the ranges studied. They obtained heat transfer coefficients up to about 20 kW/m^2-K.

It should also be noted that the research described in this thesis is the culmination of work previously introduced by Baummer et al. [28,29].

The first section of this chapter covered fundamental studies in evaporation heat transfer at the micro scale. These analyzed the performance of single or multiple

channels while changing various parameters. The second section covered various jet impingement studies where the performance of a jet was recorded across changes in various parameters. The last section covered advanced heat sink designs for which research was done to characterize their performance. The work presented in this thesis fits best into this third category, because it covers the development of a new heat transfer technology—Force-Fed Evaporation—and the evaluation of its performance. This work goes further, however, because it also demonstrates the inclusion of force-fed evaporation devices into a self-contained, two-phase system. In the following chapters, the work conducted for this thesis is described in detail. Hopefully the review reported here provides the reader with the context within which this work was conducted so as to gain a better understanding of it.

Chapter 3: Component Experimental Apparatus and Procedure

3.1: Description of the Force-Fed Process

The heat transfer method investigated in this work, force-fed evaporation, is designed to make use of the highly efficient heat transfer capable with microchannel cooling while maintaining a low pressure drop through the device. The force-fed process can be used for single-phase, evaporation, or condensation heat transfer. It uses a heat transfer surface consisting of alternating fins and channels, the channels of which are open on the top. Figure 3 shows a diagram of such a surface. To create the force-fed effect, a fluid supply header is attached to the top of the finned surface, which directs the working fluid into the micro-channels on the heat transfer surface. The header consists of alternating fluid supply channels (liquid channels in the case of evaporation) and fluid exhaust channels (vapor channels in the case of evaporation) and is oriented perpendicularly relative to the microchannels in the heat transfer surface. One such header is shown in Figure 4.

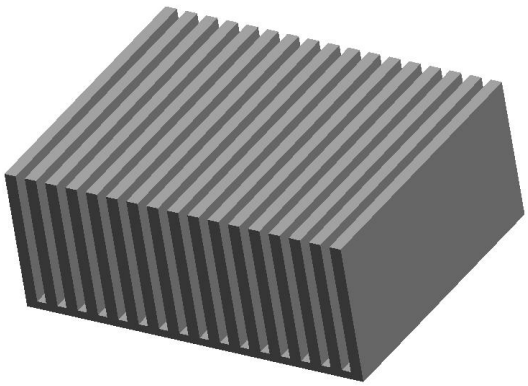

Figure 3: Diagram of Evaporator Surface

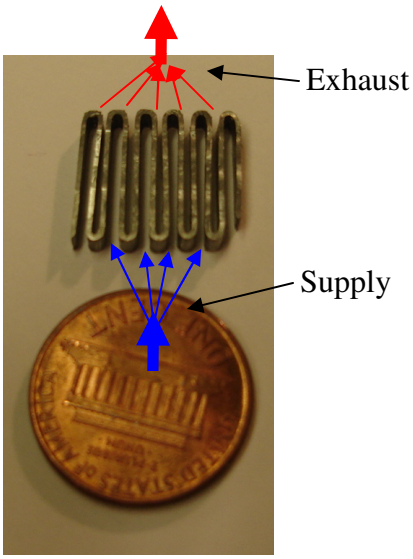

Figure 4: Picture of Fluid Supply Header

The flow pattern through the header and surface for force-fed evaporation is shown in Figure 5. The direction of view in this figure is parallel to the channels in the header and perpendicular to the microchannels in the evaporator surface. The liquid enters the microchannels by flowing down out of the header. It then evaporates as it passes a short distance through the microchannel, and the vapor flows out of the channels back into the header. The channels in the evaporator surface are effectively separated into many, much smaller channels, which all operate in parallel. The result is the formation of a liquid vapor flow pattern that supplies a liquid working fluid beneath the escaping vapor. The hundreds of microchannels operating in parallel achieve very good heat transfer with low pressure drop. For single-phase flow or condensing flow, the force-fed process works in exactly the same way, except that the fluid either does not undergo phase change, or it condenses in the microchannels for the cases of single-phase and condensation, respectively.

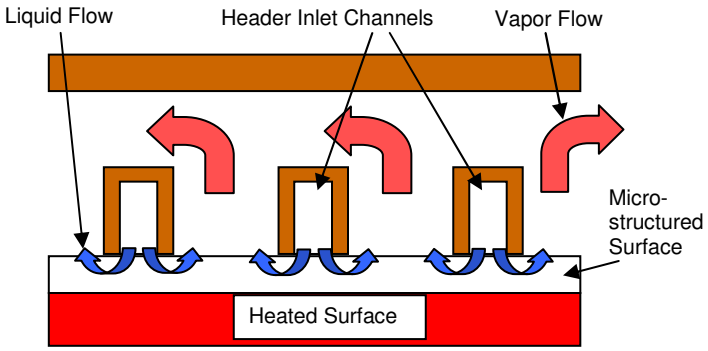

Figure 5: Force-Fed Evaporation Flow Pattern

3.2: Evaporator Design

The force-fed evaporators consist of a microchannel surface and a fluid header, as described in the previous section. The dimensions of the microchannel surfaces themselves are given in Table 1. Surface #17 was used for the component-level evaporator tests. Surfaces 11, 12, 13, 16, and 17 are used in the cold plates, which are discussed in Chapter 4. The most important parameters to note from Table 1 are the channel thickness of 42 μm, and the aspect ratio of 11.5. The small channel size provides for exceptional heat transfer, while the high aspect ratio provides a large surface area for heat dissipation. For all of the evaporator experiments, the size evaporator used was a 1 square centimeter sample.

Table 1: Dimensions of Microchannel Surfaces

Surface #	FPI	Fin Pitch (μm)	Fin Height (μm)	Channel Width (μm)	Channel Aspect Ratio (height/width)	Fin Thickness (μm)
11	100	254	889	84	10.6	169
12	143	178	406	59	6.9	119
13	143	178	610	59	10.3	119
16	200	127	406	42	9.7	85
17	200	127	483	42	11.5	85

Numerous different header styles have been used to create the force-fed effect; however, all have in common the pattern of alternating liquid and vapor channels for fluid supply and exhaust. The first-generation header, which is shown in Figure 6, consists of three inlet channels cut from brass to supply liquid to the 1 cm^2 sample. The vapor escapes from the surface though the open space between the inlet channels. Testing with this header is not a part of this work, but it is shown for reference as the first generation of this process.

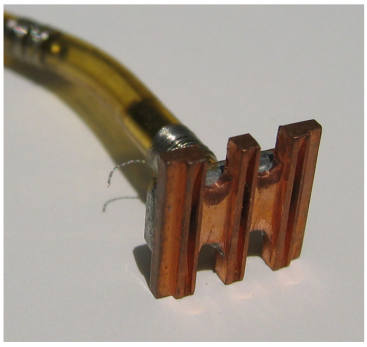

Figure 6: First-Generation Header for Evaporation

A second-generation header was also made from brass; however, it was cut from a single large block, and consists of five liquid supply channels and four vapor escape channels plus its open sides, which function as another vapor escape channel. The increased number of liquid supply channels was intended to improve heat transfer in the evaporator. Figure 7 shows this header prior to final assembly; the hose fitting on the right side of the picture was brazed to the back to connect the liquid supply line to the header.

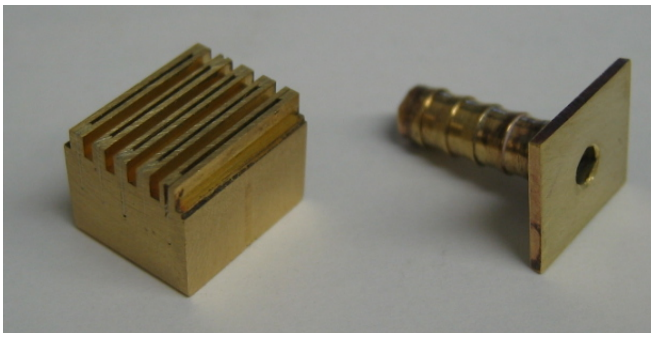

Figure 7: Second-Generation Evaporator Header

The third-generation header is the version shown in Figure 2, above. This header is made from a strip of lead-tin solder which was bent back and forth to create the desired shape. This header design has the advantage of better sealing against the microchannel surface because of the solder's softness. Also, similar headers of different dimensions can be made fairly easily due to the method of manufacture of these headers. These headers were created principally for use in the first-generation cold plate, which is discussed later, because they could also seal well against a flat top surface.

Finally, the fourth-generation header, which is shown in Figure 9, was designed solely for use in the second-generation cold plate. This header is similar to the third-generation header, except that a thin strip of copper was used rather than a thick strip of solder material. The copper was bent back and forth to create a "zig-zag" like shape as seen in Figure 8 (this figure shows a condenser header under construction; however, the evaporator header is made the same way but with fewer bends). To give the header wall its required thickness—which forces the fluid to stay in the microchannel for the desired distance—the top and bottom

quarter of the copper strip's height were bent over by 90° to create a "C" shaped cross-section. This provides a much larger flow passage in the header for vapor. The bottom part of the C keeps the microchannels sealed for a fixed distance within which the majority of the heat transfer occurs; the top of the C gives the header strength and stability. Figure 9 also shows the flow pattern through the fourth generation header.

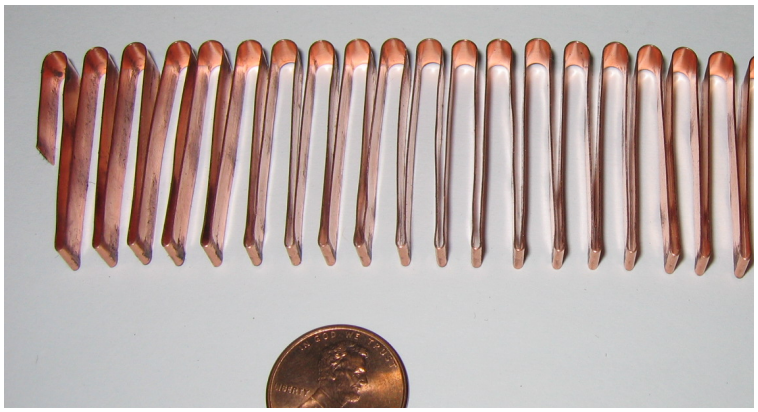

Figure 8: Top View of Fourth-Generation Header under Construction

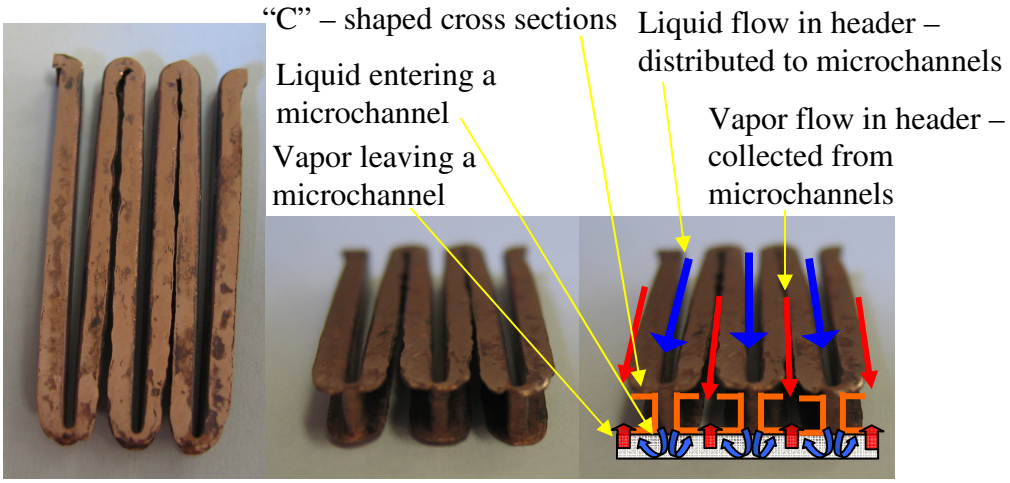

Figure 9: Top and Front View of Fourth-generation Evaporator Header

3.3: Condenser Design

As mentioned at the beginning of this chapter, the force-fed process can be applied to condensation as well as evaporation. A detailed study of force-fed condensation is not a part of this work, and has been done by another student. However, force-fed condensers are incorporated into the self-contained cold plate, so their design should be noted. The condensers in the first-generation cold plate consist of a microchannel surface of Surface #11 and a header of the same style as the third-generation evaporator headers; those in the second-generation cold plate consist of a surface of Surface #12 or #13, and are of the same style as the fourth-generation evaporator headers.

3. 4: Evaporator Test Apparatus

3.4.1: First-Generation Evaporator Test Setup

The first version of the evaporator test setup was designed for use with the first or second-generation headers described above. The primary component where the experiments take place—the test section—consists of a glass chamber containing the microchannel surface with its header, a heater assembly to provide heat to the evaporator, and the system condenser. The chamber itself consists of a glass cylinder with metal end plates all held pressed together with bolts. The condenser is built into the copper top plate, which has lines connecting the cooling water supply to the condenser and the working fluid supply to the evaporator. The lower plate is a simple aluminum plate with a hole into which the heater assembly was inserted to seal the system. The test chamber is shown in Figure 10.

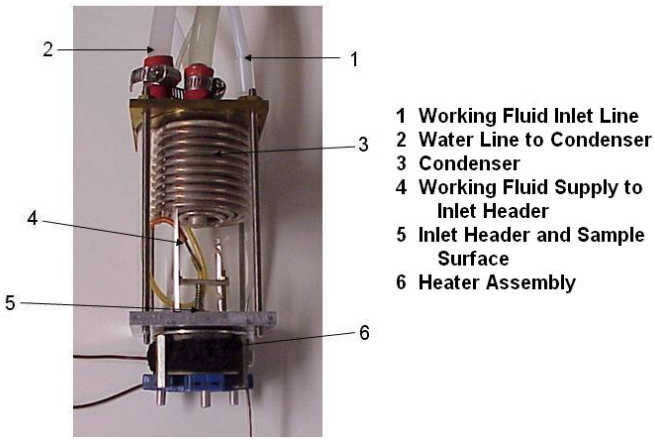

Figure 10: Experimental Test Chamber for Evaporation

The heater assembly consists of the microchannel evaporator surface and a heater that supplies heat to this surface. The evaporator is soldered onto the top of a thin nichrome diaphragm; beneath the diaphragm is a copper block which conducts heat from a heater to the evaporator surface. Surrounding the heater and copper block is foam thermal insulation. In Figure 11, the first-generation heater assembly can be seen. Bolted to the top of the evaporator surface is the first-generation header.

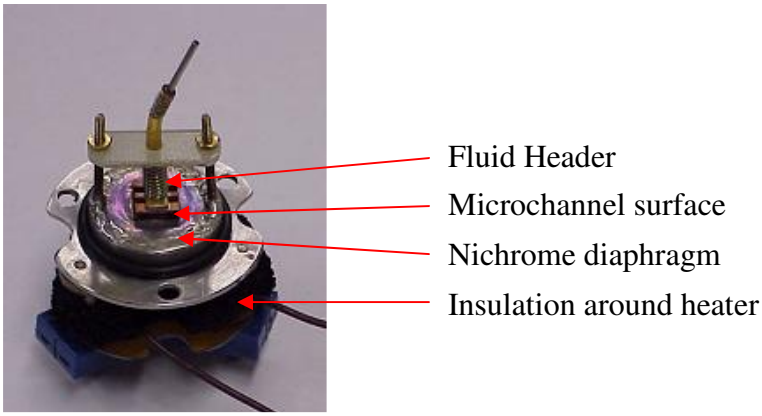

Figure 11: First-Generation Heater Assembly with Evaporator

A second-generation heater assembly was developed later to facilitate higher heat flux testing of the evaporators. This heater assembly is shown in Figure 12 without the fluid header attached. Instead of having a heater outside the chamber and separated from the surface by a diaphragm, this assembly has the heater—a 250W-rated, 1 cm^2 thin film resistor—inside the chamber. The evaporator surface is soldered directly to the heater, and Teflon surrounds the header to limit the amount of convection able to draw heat away from the sides of the heater.

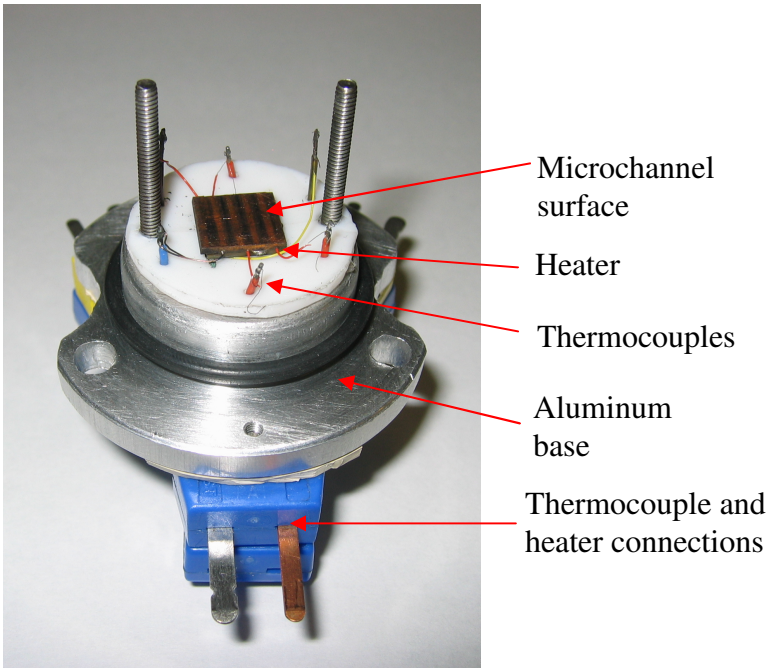

Figure 12: Second-Generation Heater Assembly

The other components of the test setup are a Neslab RTE-7 Digital Plus chiller, which supplies cold water to the condenser, a Parmer Pro-Spence gear pump to circulate the working fluid, Teflon tubes to connect this to the test chamber, a 600 W Sorenson DLM150-4 power supply to power the heater, an Agilent data acquisition device to record temperature and pressure values, and a PC running

the software Labview for data monitoring and recording. The following data measurement devices were in place: three T-type thermocouples in the heater assembly to record evaporator temperature, one T-type thermocouple in the test chamber to record fluid saturation temperature, and a Setra 280E absolute pressure transducer to measure pressure in the chamber. Flow rate was recorded directly from the pump display, as was power input from the power supply display. Later, the power supply was upgraded to a 1200 W Sorenson DSC 300-4 model and the pump was upgraded to a higher flow rate Micro-Pump™ pump for higher heat flux testing. A schematic of the first-generation evaporator test setup is shown in Figure 13.

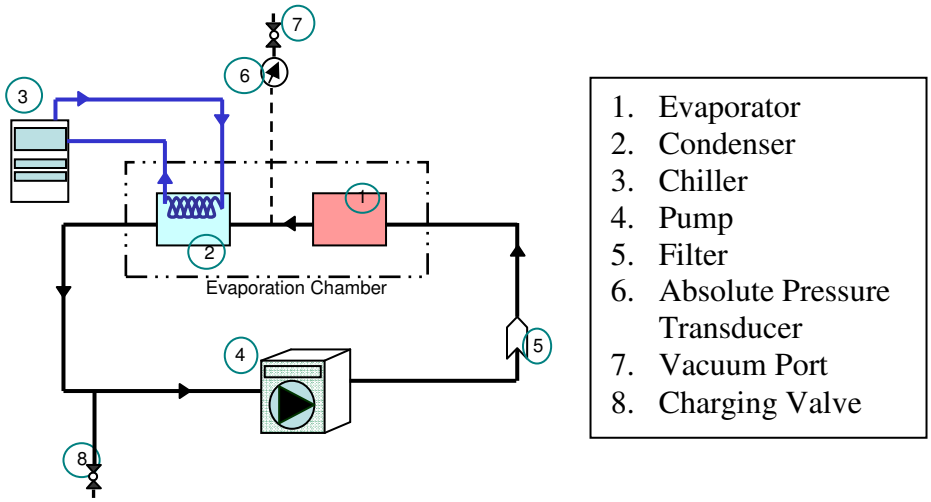

Figure 13: Schematic of First-Generation Evaporator Test Setup

3.4.2: Second-Generation Evaporator Test Setup

The second-generation evaporator test setup was designed with the goal of achieving even higher heat fluxes than those obtained with the first-generation test setup. It is built around a test section, shown in Figure 14 and Figure 15,

which looks significantly different from the first-generation test setup. This test section uses 1 cm^2 evaporator surfaces just like the first-generation test setup and uses the third-generation header design. This test section provides better instrumentation and measurement than the first-generation test setup. Because the working fluid travels from a well defined inlet to a well defined outlet, it is easier to obtain temperature and pressure measurements in those two regions. Additionally, the new test section will more easily permit sub-cooled boiling tests because the condenser comes after the evaporator test section; in the previous test section, both the evaporator and condenser were in the same chamber, which held a two-phase mixture, so the fluid sent to the pump was necessarily saturated liquid.

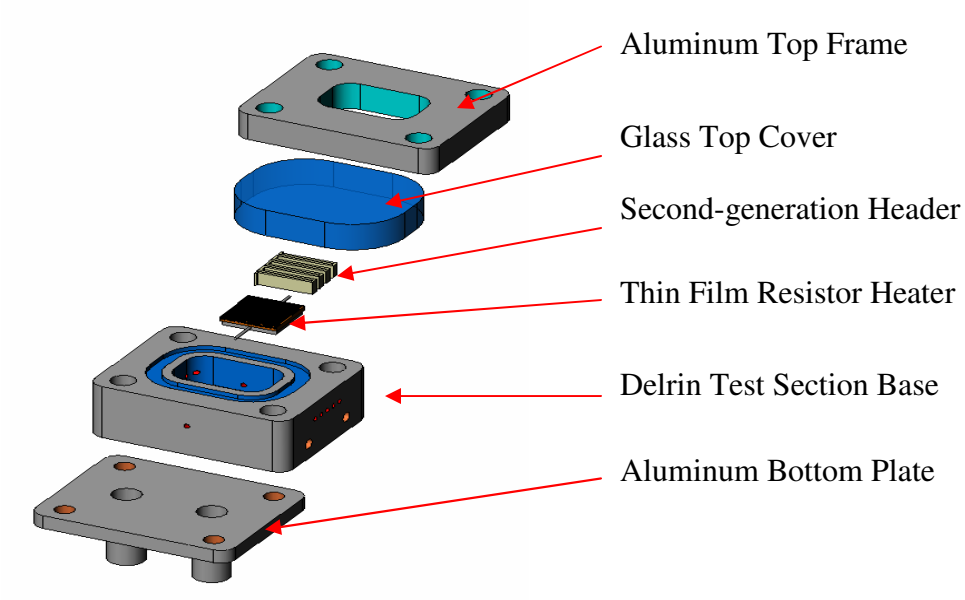

Figure 14: Second-Generation Evaporator Test Section

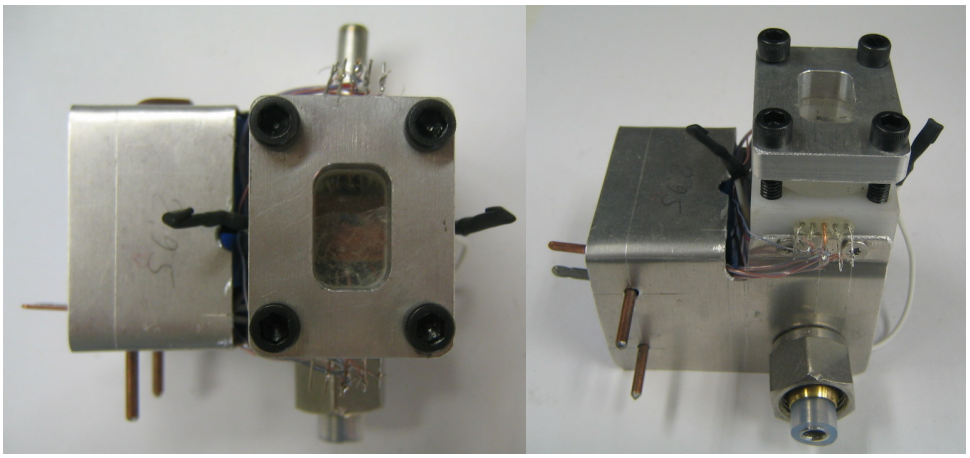

Figure 15: Top and Side View of Second-Generation Test Section

The test section described above is part of the completely new second-generation testing setup. The setup, for which a schematic and picture are given in Figure 16 and Figure 17, includes a Micro-Pump™ gear pump capable of providing a maximum of 30 ml/s flow rate. The rotometer shown in Figure 17 was replaced with a more accurate Coriolis flow meter to show the flow rate being provided for each test. Immediately before the test section, a filter is included to remove impurities in the system which could contaminate the small channels in the evaporator surface. After the test section, the vapor flows to a large plate and fin heat exchanger, which serves as the condenser, subcooler, and reservoir because of its large size. A bypass loop is present, which diverts fluid directly from the pump back to the condenser. This loop is normally closed, but it could be opened if a very high flow rate pump were to be used and if partially closing the valve on the rotometer were not sufficient to reach the desired flow rate through the test section.

On either side of the test section, plug valves are included. These allow the test section to be removed—for instance, to change surfaces or headers—without discharging the refrigerant from the entire setup. Small tubes from these valves lead to absolute and differential pressure transducers for measuring pressure drop across the test section. Also connected to the pressure transducer lines is a vacuum port, which allows only the test section to be emptied before removing or after reinstalling it. The same Neslab M75 chiller that was used in the first-generation cold plate tests provides cold water to the plate and fin heat exchanger. The 1200 W Sorenson DCS power supply used in previous evaporator tests is used to power the heater.

Data is acquired with an Agilent data acquisition system, which sends the data to a PC for monitoring and recording. Three thermocouples measure the temperature of the evaporator surface: one measures the temperature of the heater, two measure the incoming fluid temperature, and one measures the outgoing fluid temperature. Absolute and differential pressures are also monitored and recorded.

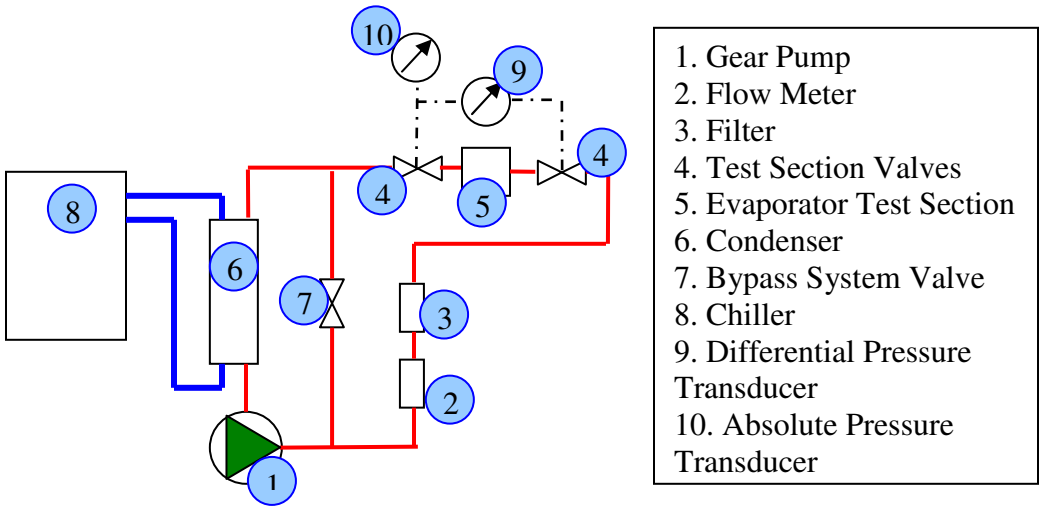

Figure 16: Schematic of Second-Generation Evaporator Test Setup

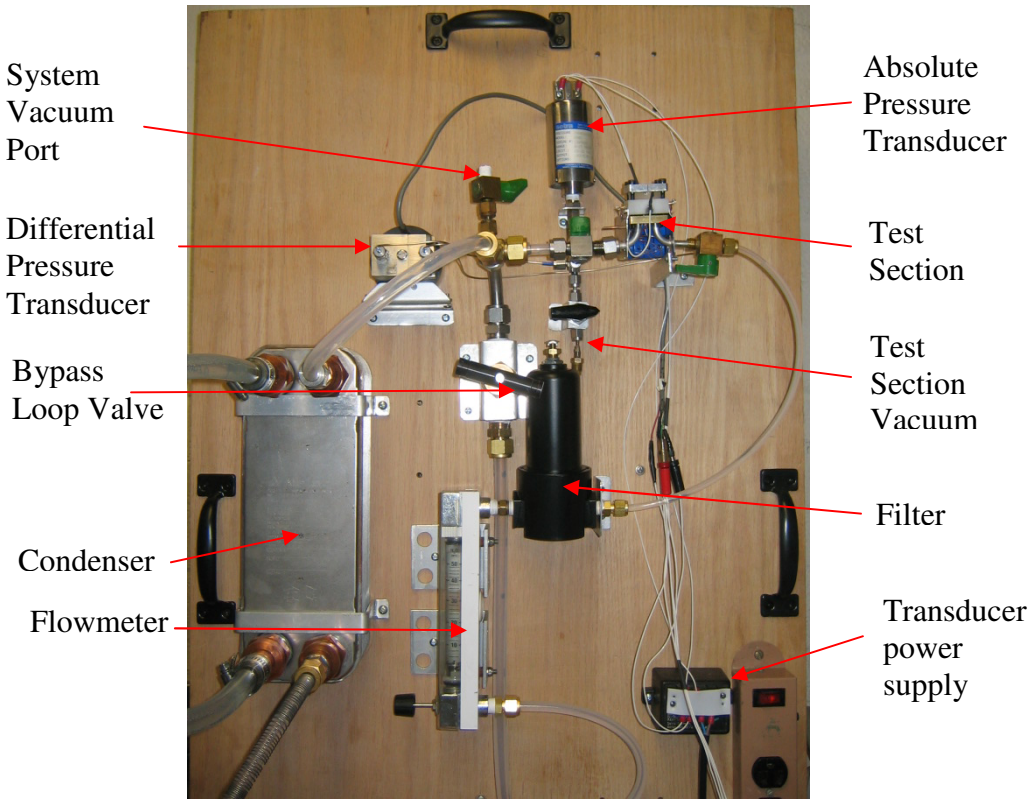

Figure 17: Picture of Second-Generation Evaporator Test Setup

3.5: Experimental Procedure

3.5.1: First-Generation Test Setup

Tests with this setup were conducted at atmospheric pressure. The working fluids used were HFE-7100 and ethanol, which have saturation temperatures of 60℃ and 78℃, respectively. The system was charged with fluid until the working chamber was approximately 20% filled, and any non-condensable gasses were purged from the system. The heater was turned on at a low power to heat the system, and the chiller temperature was set to the saturation temperature of the fluid. The saturation temperature and pressure of the fluid were constantly monitored by Labview. When both were within a predetermined margin from

their nominal values and all temperatures were stable for 4 minutes, the temperatures, pressure, and power were all recorded, and the power to the heater was automatically increased. The chiller temperature was manually adjusted as needed to keep the system temperature at its target value. When the measured values were all stable again, a new data point was recorded and the same process repeated.

This was continued until the evaporator surface temperature exceeded a predetermined safe value. This value could be exceeded by applying too much heat for the observed heat transfer coefficient, or by reaching critical heat flux, or by interrupting the liquid supply to the surface. The latter two possibilities lead to a sudden spike in temperature. Because the fluid condenses and sits in the same chamber where evaporation occurs, and because the condenser is only in contact with the vapor at the top of the test chamber, the fluid supply is always at or close to saturation temperature. Slight sub-cooling of the fluid was observed as it passed through the pump, which exchanged heat with the ambient air.

3.5.2: Second-Generation Test Setup

The test procedure for the second-generation test setup was similar to that of the first-generation test setup. The working fluid used was R-245fa, which has a saturation temperature of 15°C; therefore, tests were conducted at realistic electronics cooling temperatures rather than at a fixed pressure. The measured variables were transmitted to the computer as before; however, in place of the

semi-automated Labview system, the Agilent Benchlink software was used to monitor and record data.

To start a test, the chiller was turned on and set to a temperature of 7.5°C, below the saturation temperature of the refrigerant at atmospheric pressure. This caused the fluid entering the evaporator to be subcooled by 7-9°C. The definition of subcooling used here and throughout this project is the temperature difference from the incoming fluid to the saturation temperature (measured by a thermocouple in the vapor or two-phase region). This subcooling was used to simulate more realistic conditions, as stated above. The pump was then started to circulate fluid through the loop and through the condenser heat exchanger. This cooled down the entire system to a uniform temperature. A visual check was done to ensure that there were no bubbles caught in the pump and being sent to the evaporator. The first sets of tests were conducted to determine the effect of flow rate on the evaporator's heat transfer. For these tests, the power input to the heater was set to 50 and 200 W (500 – 2,000 kW/m^2) and the mass flux was varied from 133 to 515 kg/m^2-s. The flow rate was recorded from the readout on the Coriolis flow meter. The system temperatures and pressures were monitored on a PC, and a visual determination was made for when steady state had been reached. At this point, the data was recorded and a test at a new flow rate was begun.

For the second set of tests, the flow rate was set to an initial value and left unchanged while the heat input was increased. Power supplied to the heater was measured and recorded from the display of the digital DC power supply, while flow rate was again recorded from the flow meter readout. As before, the system was left at a constant set of conditions until the data showed that steady state had been reached. At this point the data were recorded and the power was increased for the next data point. Because of the liquid's density changes with temperature and the evaporator pressure drop increases with heat flux (due to the higher quality at the outlet of the evaporators), the flow rate actually changed during the course of this test. This creates a situation closer to what one would expect for use of these evaporators in their intended cooling application, where it would be infeasible and unnecessary to measure flow rate and make constant changes to the system during operation.

The force-fed process described at the beginning of this chapter is the fundamental object of investigation for this thesis, and as such it is found in all aspects of the project. The two generations of test setups for component-level testing of the force-fed evaporators provide the ability to determine the thermal performance of these devices. This is of interest academically, and it contributes to the development of the complete two-phase, force-fed system which follows. The next chapter provides similar information as this one but addresses the experimental setup and procedures for the system-level testing of this two-phase cold plate.

Chapter 4: System Experimental Apparatus and Procedure

In order to demonstrate the applicability of the force-fed process to electronics cooling, a self-contained, two-phase cold plate was designed, built, and tested. The goal of this project is to create a working two-phase heat transfer system capable of absorbing large amounts of heat at high fluxes in one or more regions of the plate and rejecting that heat at another location of the plate. As such, the cold plate functions as a heat spreader, cooling the hottest components of a circuit board by dissipating the heat over a larger area to a secondary heat sink. The plate should be hermetically sealed to guarantee long-term reliability and to be safe for use in electronic systems. The line replaceability of such units makes them well suited for the envisioned target applications: systems such as computer servers with large arrays of circuit boards in need of cooling

4.1: First-Generation Cold Plate

The first generation of the cold plate was designed to demonstrate a running two-phase system accepting heat from a source and rejecting it to a sink. As such, it serves as a learning tool for understanding the important parameters of such a device. It also reveals the challenges of creating a complete two-phase loop in a size-constrained package.

4.1.1: Design and Construction

As stated above, the first-generation cold plate exists to demonstrate that force-fed evaporators and condensers can be used together to create a complete two-phase

fluid loop in a small package. This plate has four evaporators, each consisting of a square piece of Surface #16, 14 mm on each side, with a second-generation fluid header on top of this. Heat is provided to each surface by a 250W-rated thin film resistor similar to those used for the evaporation test setup. There are two condensers made from 10 mm by 70 mm samples of Surface #11 and that also have the same style solder header. The condensers are each soldered to a water-cooled copper slot embedded in the cold plate. The plate was designed to use a small piezoelectric diaphragm pump. Holding all of these components together and forming the body of the plate itself is a block of Delrin, which was machined to hold the above components and provide flow passages between them. On top of the components is a glass plate that allows visualization of the flow in the plate and that is sealed by an O-ring and an aluminum frame. The dimensions of the plate are 100 x 200 mm. The plate was designed for a capacity of 500 W, with 1000 W as a stretch goal. A schematic of the first-generation cold plate is given in Figure 18, and a photograph is shown in Figure 19.

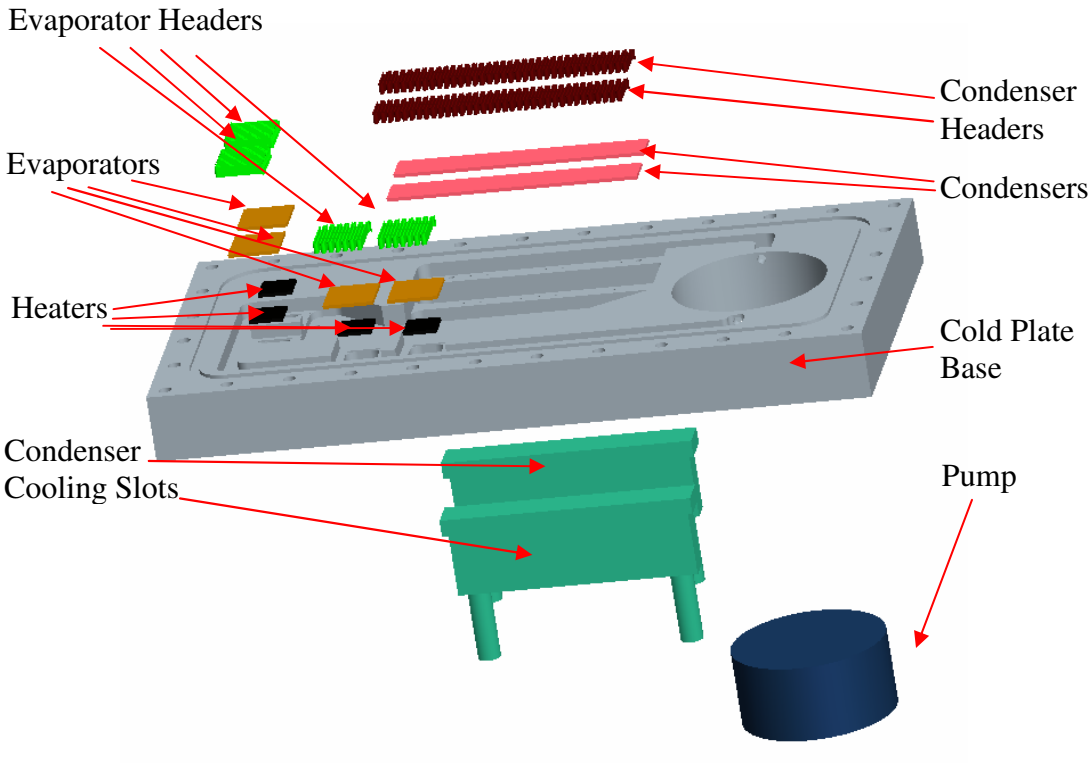

Figure 18: Diagram of First-Generation Cold Plate Assembly

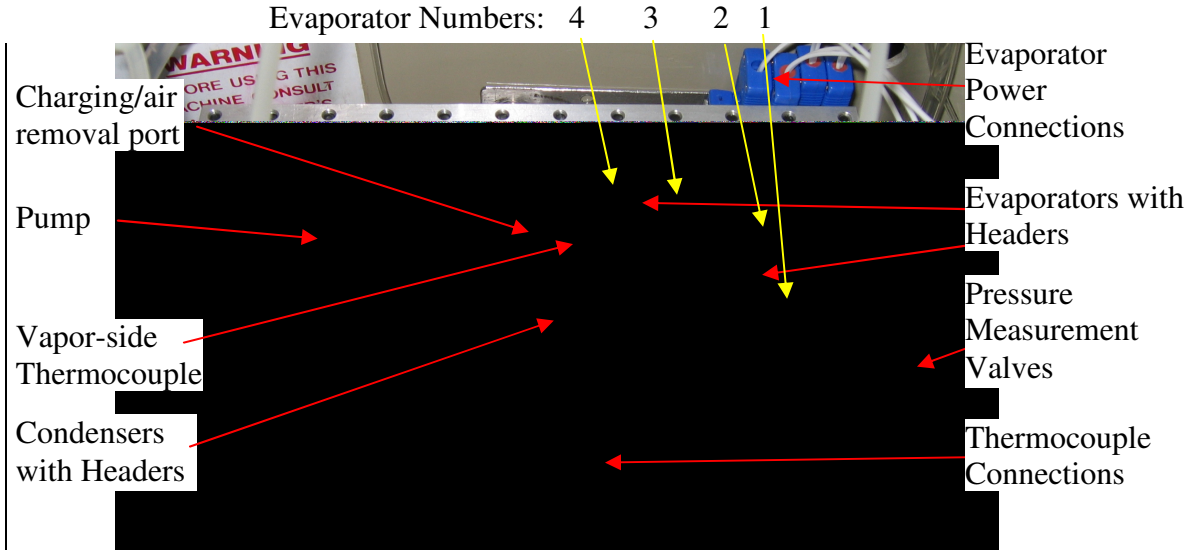

Figure 19: Photograph of First-Generation Cold Plate

4.1.2: First-Generation Test Apparatus

Because the self-contained cold plate represents a complete two-phase fluid loop, it holds within itself most of the components of a test setup. All that is required is to supply chilled water to the condensers and power to the resistors, and to hook up measurement equipment. To accomplish this, an experimental test setup was constructed that includes four independent variable transformers to serve as power supplies for the four resistors, a Neslab M75 chiller to provide cold water, absolute and differential pressure transducers, thermocouples, and an Agilent data acquisition system to monitor the data and send it to a PC, where it is recorded. A picture of the test setup is shown in Figure 20. The system has a total of 23 thermocouples. Two are embedded in the back side of each evaporator microchannel surface; five are placed on the back side of each condenser; and one each measures the temperature of the following: two-phase refrigerant mixture, condensed refrigerant, cold water into the first condenser, cold water between condensers, and cold water after second condenser. A bracket to hold all of these thermocouples was built onto the side of the cold plate and can be seen in Figure 19. The pressure in the plate is measured at eight locations: before and after the first and last evaporator, and before and after the two condensers at two locations each. Rather than use eight pressure transducers to monitor each of these locations, one absolute and one differential transducer were used. A series of 3-way valves, which can be seen in Figure 19, connected one location at a time to one side of the differential transducer, while the other side was always connected to the same location as the absolute transducer.

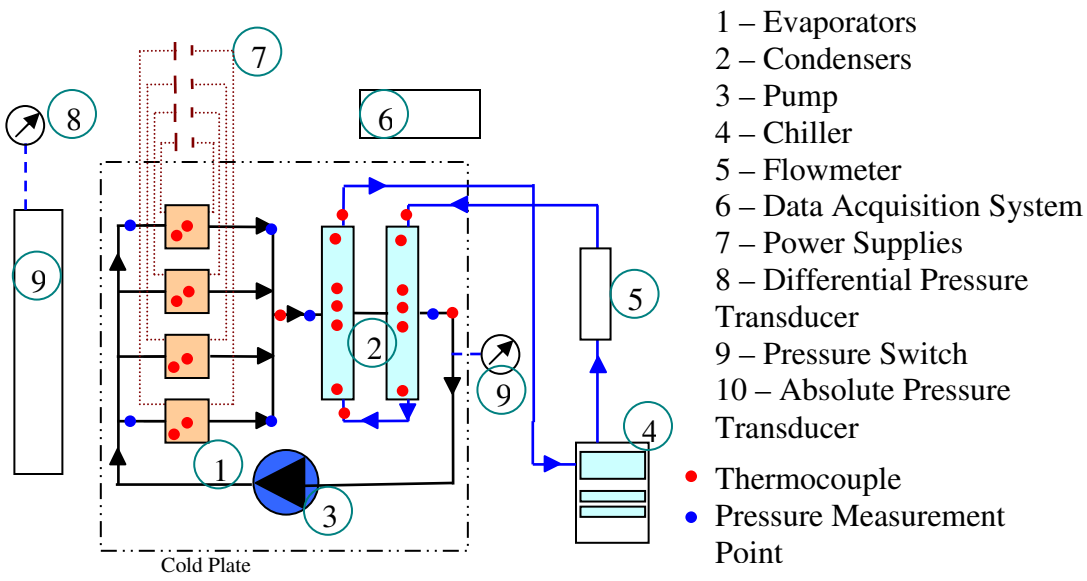

Figure 20: Schematic of First-Generation Cold Plate Test Setup

Because of difficulties encountered with the piezoelectric pump, which are discussed in Chapter 6, a different pump was later used, which was situated outside the self-contained cold plate. The pump is a model 300-A micro-gear pump manufactured by Flight Works, Inc. (Mission Viejo, CA), as a turbine fuel supply pump. To connect it to the plate, the top of the piezoelectric pump was removed and two pipe fittings were attached to it. Flexible tubes were run from these fittings to the gear pump which was external to the cold plate. In this way, the piezoelectric pump body remained in place, and continued to seal the plate, while the gear pump provided the actual pumping power. Using the pumps in this arrangement means that the cold plate was no longer truly self-contained because the operating pump was external to it, however, the gear pump is smaller than the piezoelectric pump, so the plate could have included this pump internally, had it been designed for it. A reservoir was also later added to the test setup between the condenser and the pump. This also violated the "self-contained" nature of the

cold plate; however, its presence was necessary to run the system to discover how the cold plate system behaves; additionally, the reservoir itself was a learning tool, as it led to the incorporation of a reservoir in the second-generation cold plate, as described later.

4.1.3: First-Generation Experimental Procedure

Tests were conducted with HFE-7100 and with a mixture of 30% methanol-70% water. Before each experiment, the system was charged with refrigerant, and non-condensable gasses in the system were evacuated. To start each test, the pump was set to approximately its maximum flow rate of 800 mL/min. Specific recording of the flow rate was difficult because the pump's pressure-voltage-flow rate curves do not include such low pressures as are found in this system, and the cold plate—being an application demonstration—did not include a flow meter. The evaporators were turned on at roughly equal power levels, and the chiller was turned on to pump cold water to the condensers. When the system reached steady state—as determined by observing changes in the measured variables—the data were recorded, and the evaporator power was increased. The temperature of the chiller water was adjusted manually to keep significant sub-cooling of 8-17℃ (HFE-7100) in the liquid side of the system. This was necessary to get the best possible system capacity and to reduce the occurrence of vapor bubbles in the liquid lines. The difference in subcooling between the different experimental setups was caused by the procedure (constant or variable cooling water temperature) and the effectiveness of the condensers rather than by refrigerant properties. The pressure of the system was permitted to fluctuate naturally for the

different power input levels, which is a more realistic simulation of the plate's operation in the target application.

4.2: Second-Generation Cold Plate

After the first-generation cold plate demonstrated the viability of a self-contained, two-phase cold plate system, a second-generation cold plate that brings this cold plate concept closer to marketability was created. Though the plate was not designed with the ability to cool an external heat source—such as an electronics board—small design changes could be made within the existing design concept that would make this possible. This plate has been designed with real-world usability in mind. For this reason, the main plate components are all constructed with mass production style processes such as stamping and folding.

4.2.1 Design and Construction

The second-generation cold plate differs significantly from the first in its fundamental design framework. The first-generation plate consisted of several components placed inside cavities cut into a monolithic block that had been custom shaped by milling. By contrast, the second-generation plate consists of components that are each packaged as independent modules. These modules are arranged on a flat brass plate whose purpose was only to hold the modules together. This design provides a significant increase in flexibility because the modules can easily be moved around on the plate to tailor the system to various applications. This method also provides an improvement in terms of flow distribution, which is discussed below.

The first of the cold plate components is the evaporator module. This module, seen in Figure 21, consists of a microchannel surface 17x34mm in size and a fourth-generation fluid inlet header sealed in a stamped copper box. Copper tubes are attached to provide for fluid inlet and outlet to the component. The module shown in Figure 21 also includes two 1-cm^2 heaters with three thermocouples to measure the temperature of each. Figure 22 shows a partially assembled evaporator module in which the microchannel surface and header can be seen.

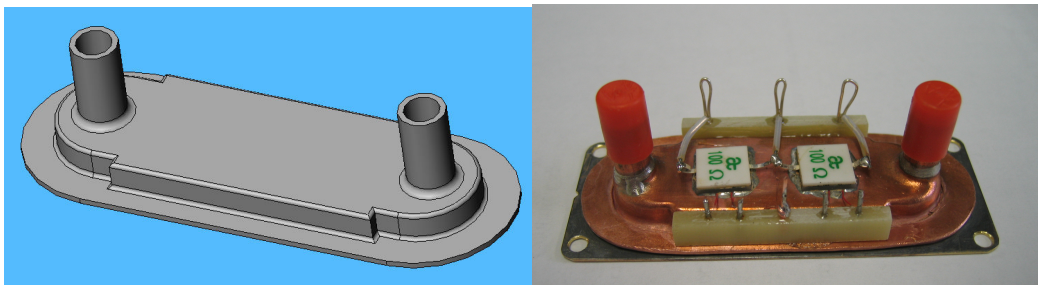

Figure 21: Diagram and Picture of Cold Plate Evaporator Module

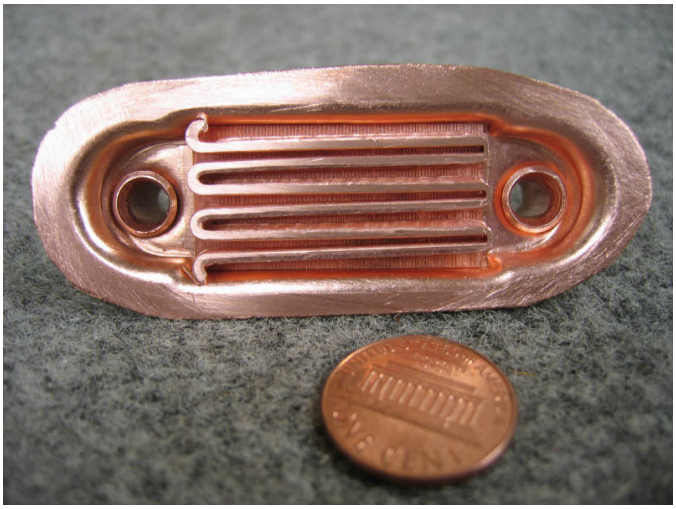

Figure 22: Picture of Partially Assembled Cold Plate Evaporator Module

The second primary component of the cold plate is the condenser module, shown in Figure 23. Like the evaporator module, the condenser module consists of a microchannel surface and a header sealed in a copper box; however, the condenser is much larger, with a surface size of 34x135mm. A large condenser is possible because the condenser does not need to be tailored to the hotspots of a specific application, making small size unnecessary. Additionally, the overall area for condensation is larger because for a given condensation heat transfer coefficient, a larger area means the working fluid can be held at a lower temperature. Because the condensers are larger and fewer in number, they each accept vapor from three evaporators through the three inlet tubes to the condenser.

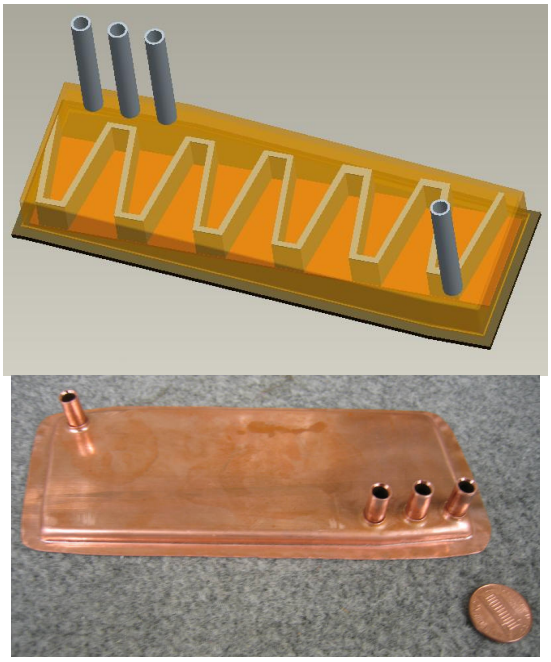

Figure 23: Model and Picture of Cold Plate Condenser Module

The two other components of the cold plate are the pump and the reservoir. The pump, shown in Figure 24, is a magnetically-coupled impeller pump manufactured by Laing, Inc. This pump is hermetically sealed because of the

magnetic coupling between the motor and the impeller, and it can provide up to 25 l/min flow rate or 27 kPa pressure. A reservoir, shown in Figure 25, is included to separate any vapor that leaves the condenser from the liquid being supplied to the pump and to provide the pump with liquid during the transient start-up condition. The reservoir is a stamped copper box similar to the ones used in the evaporator and condenser modules. The fittings visible in the picture below are the liquid inlets from the condensers; the outlet is from the bottom of the reservoir to ensure that only liquid is drawn from it.

Figure 24: Picture of Impeller Pump

Figure 25: Picture of Stamped Reservoir

The complete model created for the second-generation cold plate is shown in Figure 26. It consists of eight evaporator modules along one edge with three condensers in the center and a pump and reservoir along the far side. The overall dimensions of the plate are 200x400 mm. As mentioned earlier, the purpose of the cold plate is to function as a heat spreader; the system absorbs heat at a high heat flux at the evaporators and dissipates it to a water heat sink over a larger area. Thus, in order to function for any size electronics board, the plate must absorb heat from one side and dissipate it to the other. To accomplish this, the evaporators are heated from above, as seen in Figure 21, whereas the condensers are cooled from below, through the brass plate holding the system together.

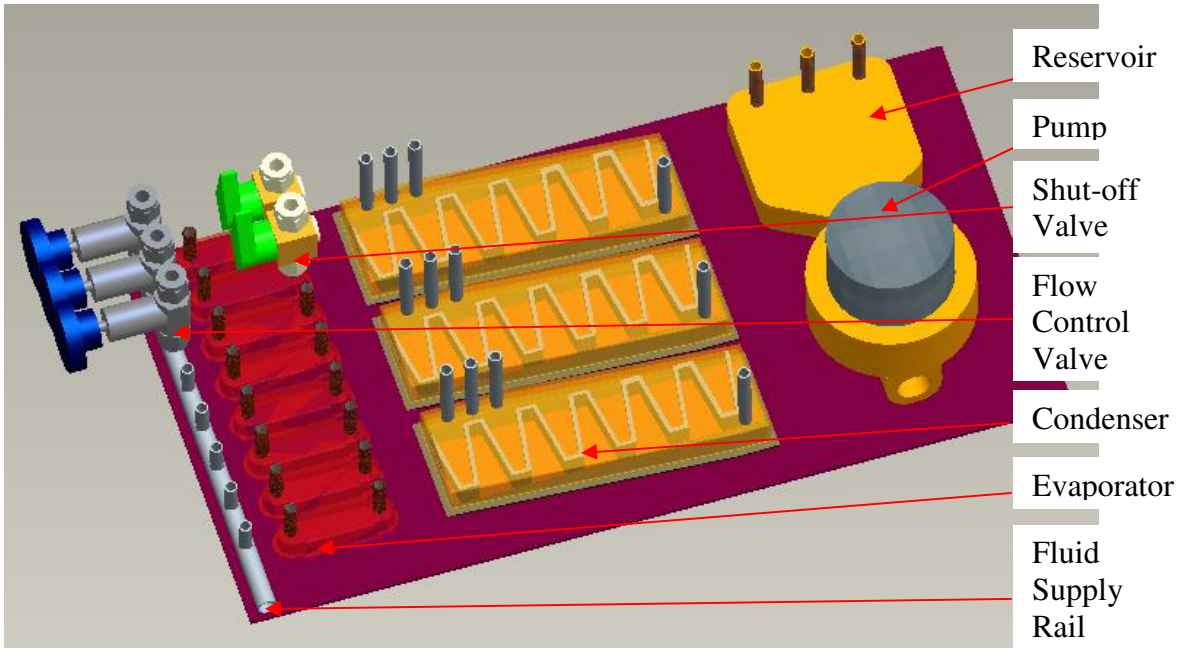

Figure 26: Model of Second-generation Cold Plate System

It is clear from Figure 26 that the current generation of this system is not designed to cool an actual electronics board; rather it functions as a more advanced demonstration of the concept. Specifically, the main reason this plate cannot work for the application is that the top side that faces the heat source has numerous pipes and valves protruding from it. In this version of the cold plate, the components are all connected with Teflon tubes by means of these fittings. This allows more flexibility in testing the cold plate system in different ways. The valves are used to customize the pressure drop to each evaporator in order to create equally distributed flow.

A minor modification to the existing design would allow this system to function in its intended application: all of the tubes could be replaced with stamped copper channels sitting flat on the surface of the cold plate. This would require only a

modification to the shape of the stamped evaporator and condenser packages so as to enable them to accept a horizontal copper channel rather than a vertical tube. Additionally, the valves could be replaced with channel constrictions with fixed pressure drops to mimic the effect of the valves. Figure 27 shows a picture of the test-assembled cold plate. The number of evaporators and condensers has been reduced to 6 and 2, respectively, for the first tests. If necessary, the flexibility of the design allows two more evaporators and one more condenser to be added where there is presently empty space. Additionally, the isolation valves at the evaporator outlets have been omitted, because they were determined not to be necessary for the scope of tests in the present work. Finally, Figure 28 shows a picture of the fully assembled cold plate with all testing instrumentation attached.

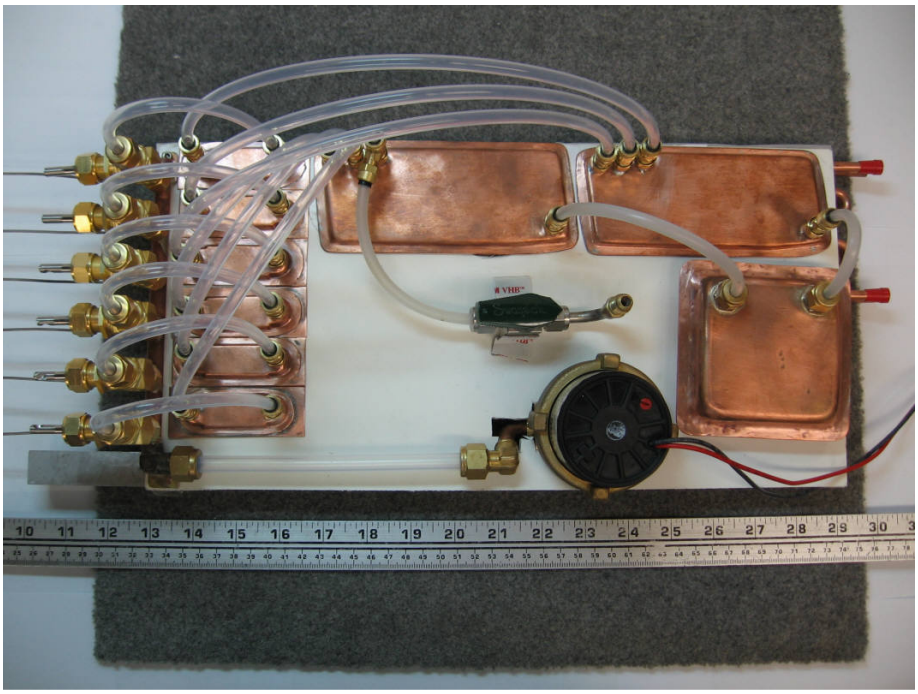

Figure 27: Picture of Test Assembled Second-Generation Cold Plate

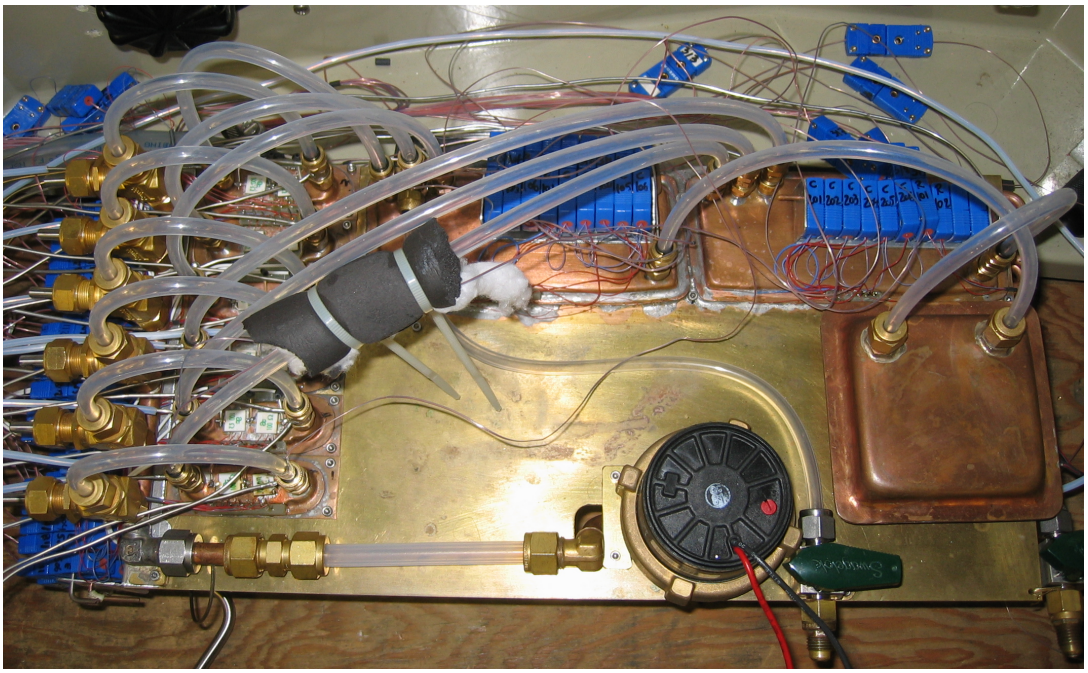

Figure 28: Picture of Finally Assembled Second-Generation Cold Plate

4.2.2: Second-Generation Test Apparatus

Like the first-generation cold plate, this second-generation cold plate contains within itself the primary elements of the test apparatus. To accommodate the higher power capacity of this design, several variable AC transformers were used to power the heaters on the evaporators. Cold water was supplied by the same Neslab M75 chiller that was used in the tests of the first-generation cold plate. Heat absorption from the condensers was accomplished by piping this water through a CP15G05 plate-and-tube heat exchanger manufactured by Lytron, Inc (Wobburn, MA), which is shown in Figure 29. The flow rate to this device was measured with a Coriolis flow meter.

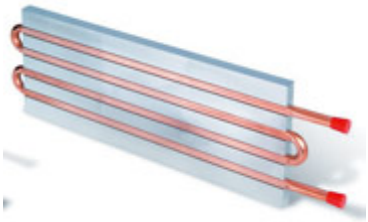

Figure 29: Picture of Plate-and-tube Heat Exchanger. Adopted from [30]

As before, absolute and differential pressures were measured in the cold plate system. Because of the larger number of components compared with the first-generation cold plate, the temperature and pressure were measured in more locations. Thermocouples were placed in the following locations: 3 on each heater on each evaporator, 6 on each condenser surface, 3 in the working fluid in the supply rail, and 3 at the pump inlet, for a total of 54.

To accommodate the larger number of pressure measurement locations, a "pressure switch" was used. This is a 32-way valve that can individually connect any of 16 pairs of connection ports to a pair of central connection ports. An absolute and a differential pressure transducer were connected to these central ports to measure system pressures. Using this arrangement, pressure was measured on both sides of each evaporator and condenser and before the six throttling valves. The use of these locations also allows measuring of the pressure drop across each valve, which could be used to develop a plate with balanced flows without valves as described at the end of Section 4.2.1. Pressure connections to the cold plate were made by drilling and brazing a small metal tube into the fittings at the inlet or outlet of the various components.

Pump power was measured by recording the voltage and current supplied to the pump. As with the first-generation cold plate, measurements of temperature, pressure, pump power, and evaporator power were collected by the Agilent data acquisition system and communicated to a PC for monitoring and recording. Connections to the plate were included to allow vacuuming and charging of the plate.

4.2.3: Second-Generation Experimental Procedure

The goals of the second-generation cold plate system tests were the same as for the first-generation plate, and so the procedure for testing is similar. Prior to testing, the system was evacuated of all gasses and filled with the refrigerant R-245fa, which was also used for the second-generation evaporator tests. The pump, which has an adjustable flow rate, was set to its maximum flow rate, and the chiller was turned on to supply water at 5°C to the plate-and-tube heat exchanger, which produced 7-9°C of subcooling. The throttling valves leading to the evaporators were left 100% open for all tests. Their use—for equalizing the flow across all evaporators—is left for later work. The variable transformers were turned on to set the evaporators to an initial, equal power level. Throughout the tests, the power level continued to be equally distributed across the evaporators. The initial power level for the plate was 900W, which corresponds to 750 kW/m^2. This power level was held until all system parameters were constant. A data point was recorded, and the pressure switch was used to gather the necessary pressure data. The power level was then increased approximately

300W, and the system was allowed to reach steady state again. Because the transformers powering the evaporator heaters are not identical, they maxed out at different powers. Above 1660 W, the evaporator powers were no longer balanced, so the last data point was captured with all heaters maxed out at different power levels.

The first-generation cold plate described in the first half of this chapter represented the first attempt to integrate into a complete system the evaporators that were studied in the original tests. As a learning tool, it produced a wealth of information, which led to the design of the second-generation cold plate. The improvements incorporated into this second system allowed it to function very well and provide additional data. The following chapter provides the test results for the evaporator components that went into these systems, and Chapter 6 presents the test results and discussion about the cold plates themselves.

Chapter 5: Component-Level Results and Discussions

5.1: First-Generation Evaporator Test Setup

Tests were conducted with the first-generation evaporator test setup as described in Chapter 3. As mentioned in that chapter, testing with the first-generation header was not a part of this work, so all results shown in this section were obtained with the second-generation header. The first tests were conducted using HFE-7100 as the working fluid. The mass flux was fixed at 362 kg/m^2-s throughout the test. The data collected, shown in Figure 30 and Figure 31, show that the evaporator can dissipate over 3,000 kW/m^2 at a heat transfer coefficient of 62.5 kW/m^2-K. The highest heat transfer coefficient during the run was 87.3 kW/m^2-K. The first run of this experiment ended when dryout occurred, causing a sudden spike in the temperature of the heater before the power was turned off.

The second and third runs of this experiment produced similar results, but with lower temperatures across the board, which correspond to higher heat transfer coefficients. Because Run 3 so closely matches Run 2, and these do not match Run 1, it was suspected that overheating the heater assembly caused some damage to it. It is believed that the Teflon insulation on the thermocouple wires burned away where the wire is embedded between the heater and the microchannel surface. This would cause a thermocouple junction to form closer to the edge of the evaporator, which would cause the thermocouple to report the cooler temperature there. Therefore, it is believed that Runs 2 and 3 provide sound

qualitative results, but do not necessarily show data that is quantitatively better than Run 1.

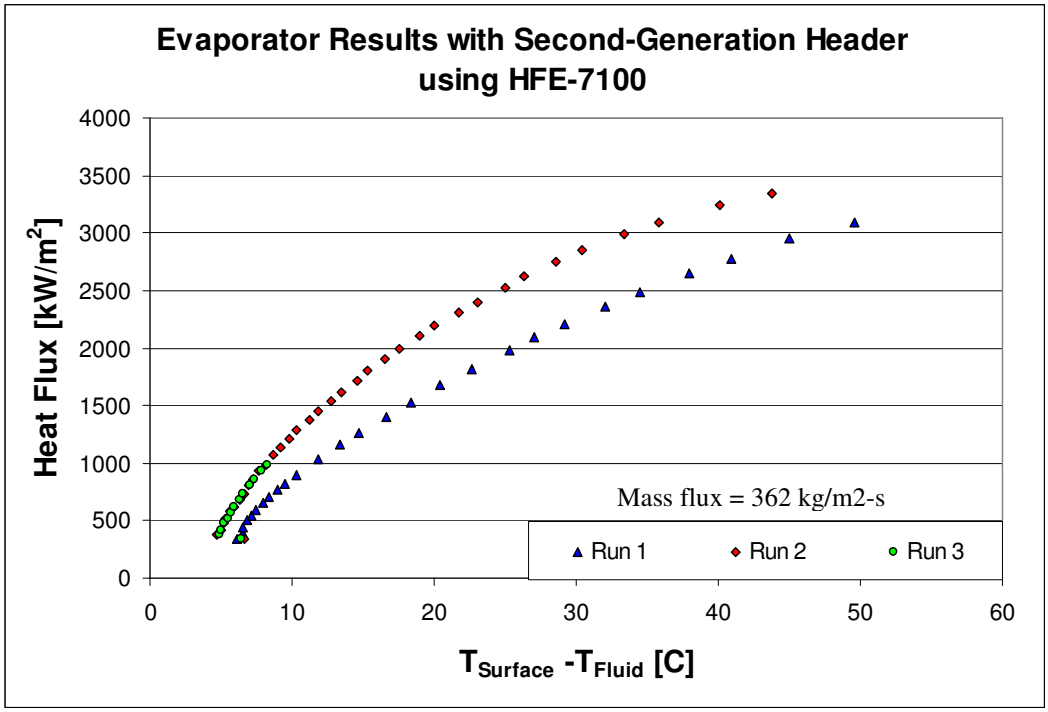

Figure 30: First-Generation Evaporator Results with HFE-7100

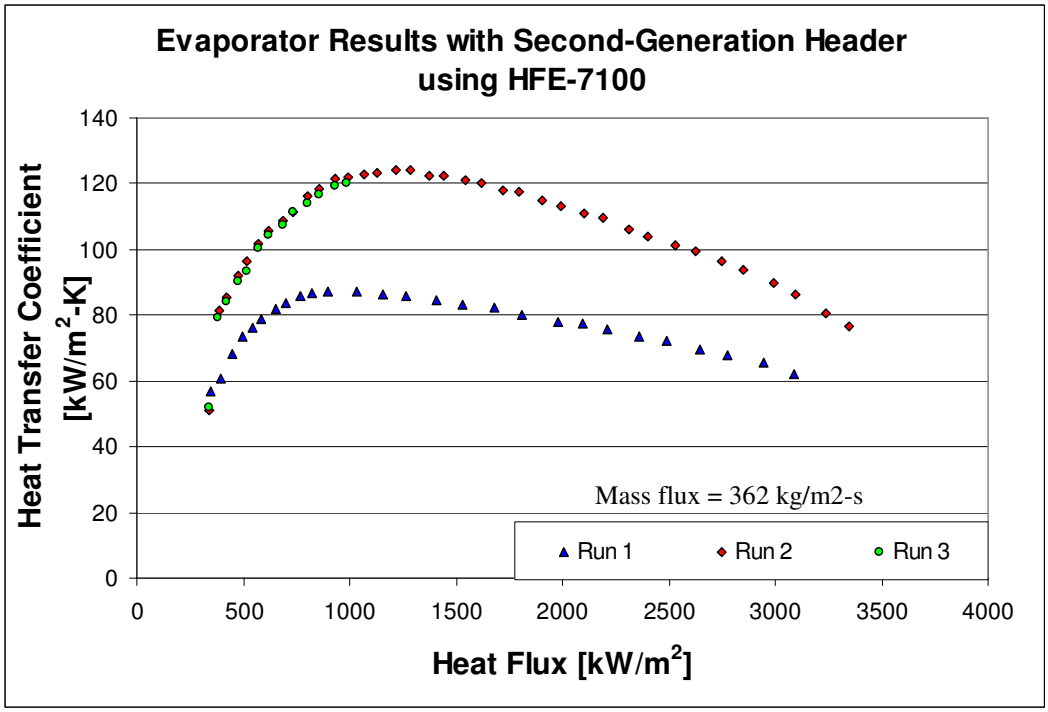

Figure 31: First-Generation Evaporator Results with HFE-7100

After conducting the above tests with HFE-7100, the test setup was used with ethanol. Because of ethanol's higher boiling point, these tests were conducted at a higher fluid temperature. The results of these tests are shown in Figure 32 and below. As with Runs 2 and 3 above, it is believed that the thermocouples in these tests were not measuring the highest temperature in the device. Again, the data below can be considered to give a qualitative description of the performance of the force-fed evaporators with ethanol relative to HFE-7100. Additionally, the maximum heat fluxes remain valid in these tests. Run 1 with ethanol produced a heat flux exceeding 4,000 kW/m^2. The nominal maximum heat transfer coefficient in this test was 300 kW/m^2-K compared to 120 kW/m^2-K for Run 2 of the HFE-7100 test. Run 2 of the ethanol test produced a similar data set, with slightly lower overall performance. In both data sets, one can see a sudden

decrease in the surface temperature after the first few data points, which appears to indicate the onset of boiling. Run 2 was not carried out all the way to the maximum of Run 1 because it was realized that the ethanol was dissolving the resistor material of the heater. This made stable power levels unattainable and prompted a destructive examination of the test setup.

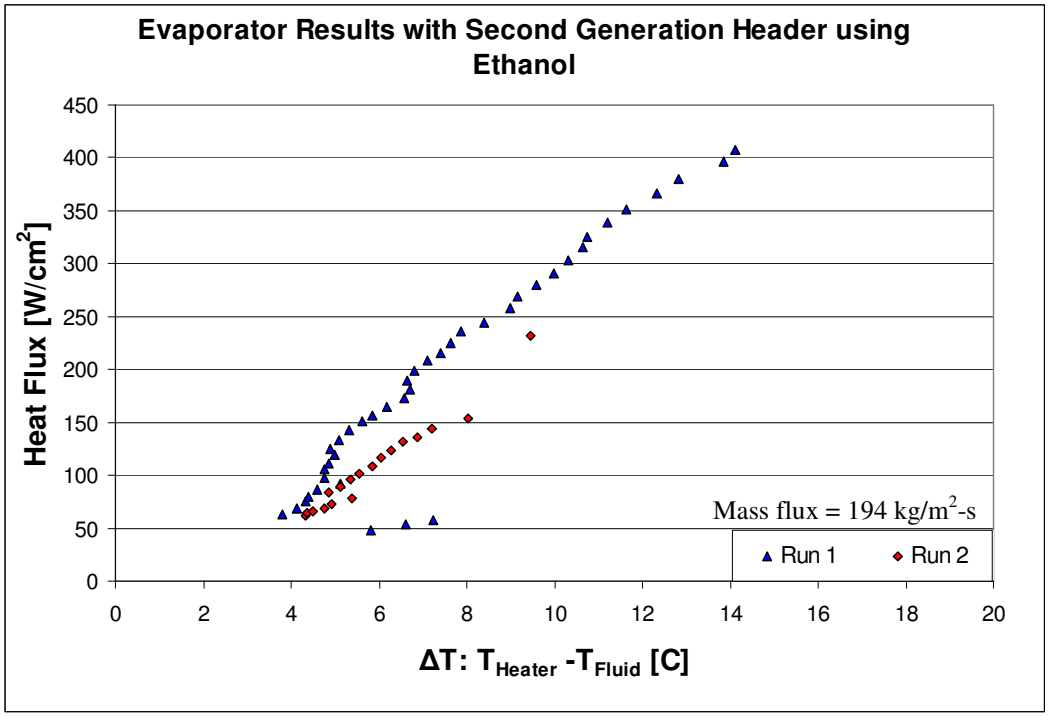

Figure 32: First-Generation Evaporator Results with Ethanol

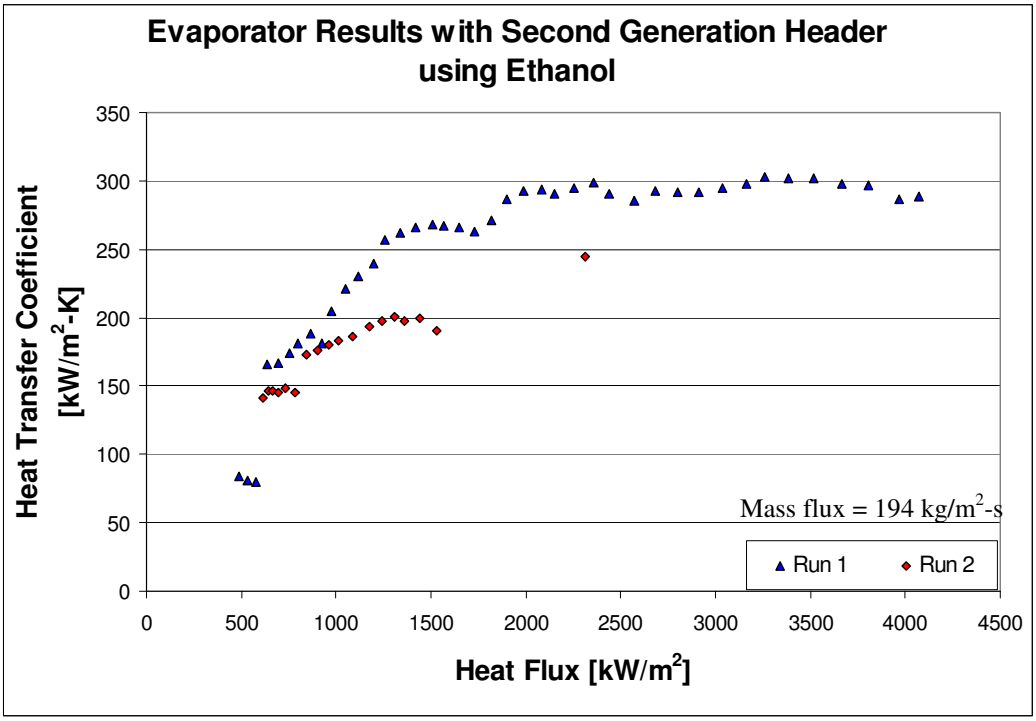

Figure 33: First-Generation Evaporator Results with Ethanol

After the above tests, the heater assembly was repaired with a new heater and thermocouples for the purpose of testing the second-generation header at a much higher flow rate of HFE-7100. Additionally, it was suspected that the hard brass surface of the heater did not perfectly seal against the microchannel surface. To improve sealing, the header was coated with a layer of solder. Figure 34 and Figure 35 show the results of this test along with the results of Run 1 of the HFE-7100 tests for comparison. The results of this test stand out because the maximum heat flux obtained was an unprecedented 9,240 kW/m^2. This was obtained with a heat transfer coefficient of 160 kW/m^2-K.

The other salient aspect of this data is the shape of the heat flux vs. temperature plot. It resembles the traditional plot for pool or flow boiling on a flat plate,

which begins with a low, linear section near the beginning where all the heat transfer is by single-phase convection. After this there is a slight drop in temperature at the onset of boiling, and then the heat flux climbs steeply with increasing temperature as nucleate boiling dominates the heat transfer. The fact that no bubbles were observed in the evaporator outlet prior to 5,000 kW/m^2 suggests that this may be exactly what is shown in Figure 34. The drop in temperature occurred later, at 7,000 kW/m^2; however, it may be that true nucleate boiling did not begin until then.

This experiment was stopped when the failure of a tube in the pump assembly caused momentary dry-out on the evaporator surface. At such a high heat flux, this dry-out immediately caused the surface to overheat and the heater to be destroyed. The shape of Figure 34 suggests that the nucleate boiling regime might have continued to even higher heat fluxes had the dryout not occurred. This experiment was not repeated because the second-generation evaporator setup was already in development, and it was expected that this could give similar performance with better instrumentation.

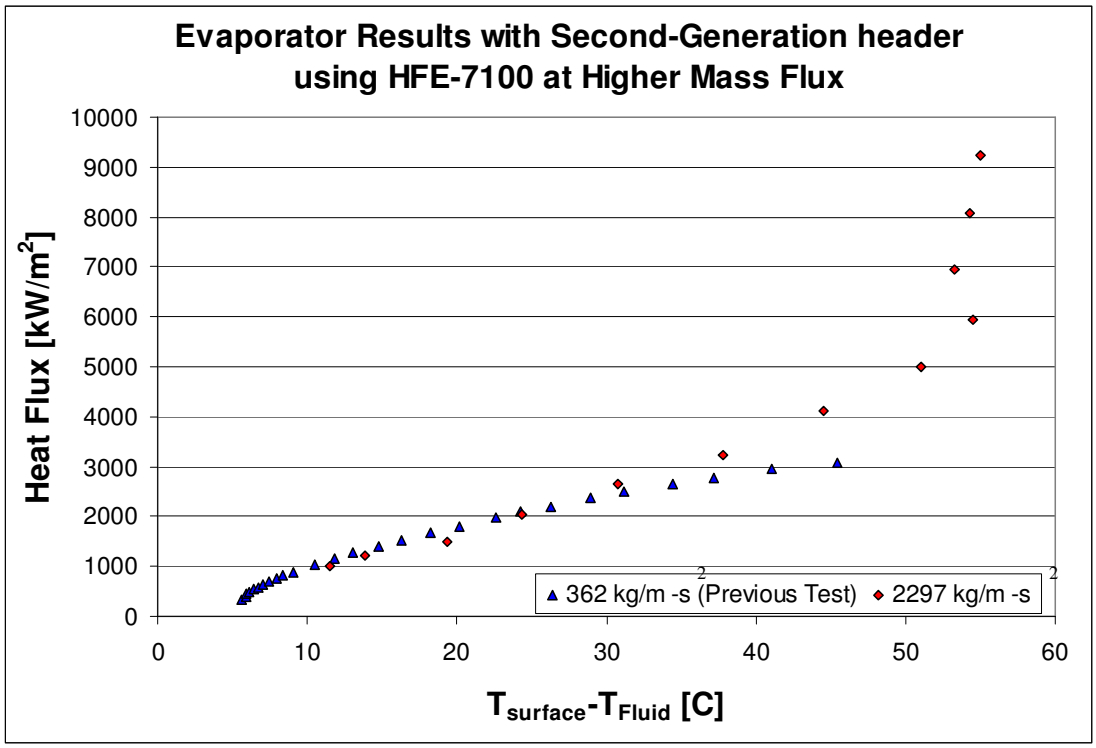

Figure 34: First-Generation Evaporator Results at Higher Mass Flux

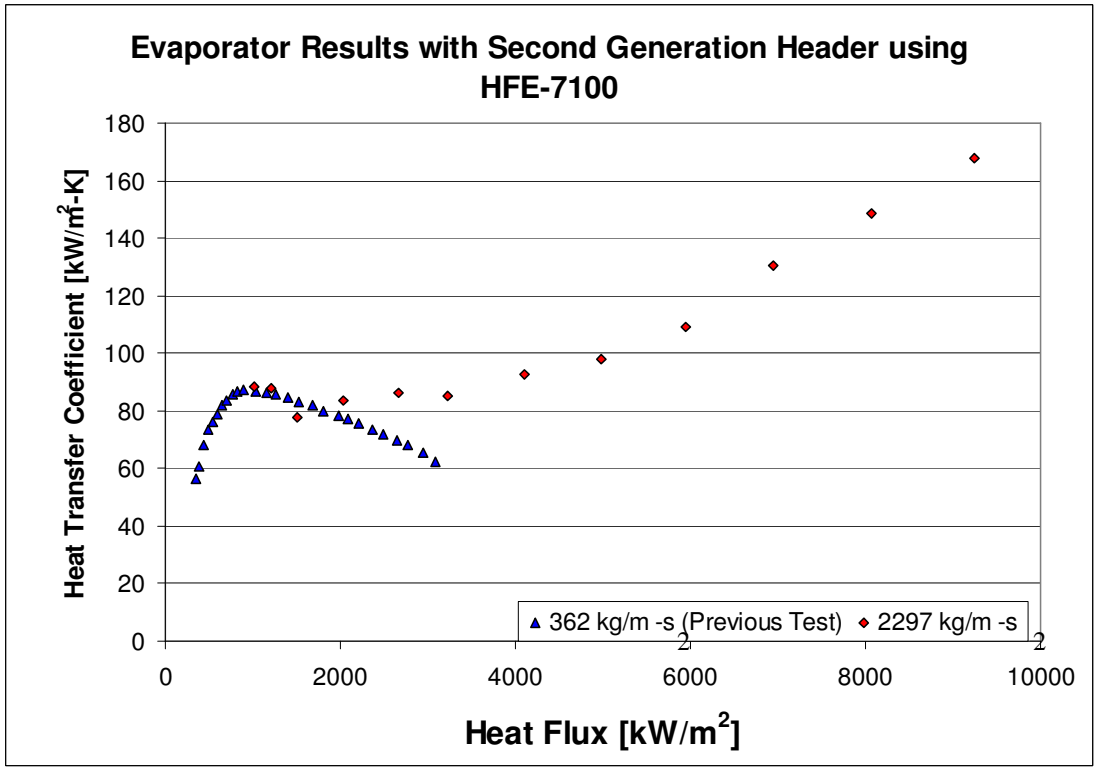

Figure 35: First-Generation Evaporator Results at Higher Mass Flux

5.2: Second-Generation Evaporator Test Setup

As described in Chapter 3, the second-generation evaporator test setup was developed with the expectation of attaining improved performance coupled with better process measurement. Two types of tests were performed with the new setup: constant power tests and constant mass flux tests. The constant power tests were conducted at 500 kW/m^2 and 2,000 kW/m^2. These levels where chosen lower than the best performance achieved in the first-generation evaporator test setup so that the evaporators could dissipate the required heat load even at low mass fluxes. The mass flux for these tests ranged from 133 to 515 kg/m^2-s. Due to the system configuration, the pump could not produce the much higher mass flux seen in the final tests with the first-generation setup. The results of this test, shown in Figure 36, convey an unexpected outcome. At 2,000 kW/m^2, the heat transfer coefficient increases slightly with increased mass flux; however the curve becomes increasingly flat at higher mass fluxes. At 500 kW/m^2, the heat transfer coefficient decreases slightly and then levels off, which is the opposite of what one would expect based on first-generation results, in which a much higher mass flux produced much better performance. The performance was similar between the two power levels, which matches the first-generation data, which showed no uniform trend of performance with respect to heat flux.

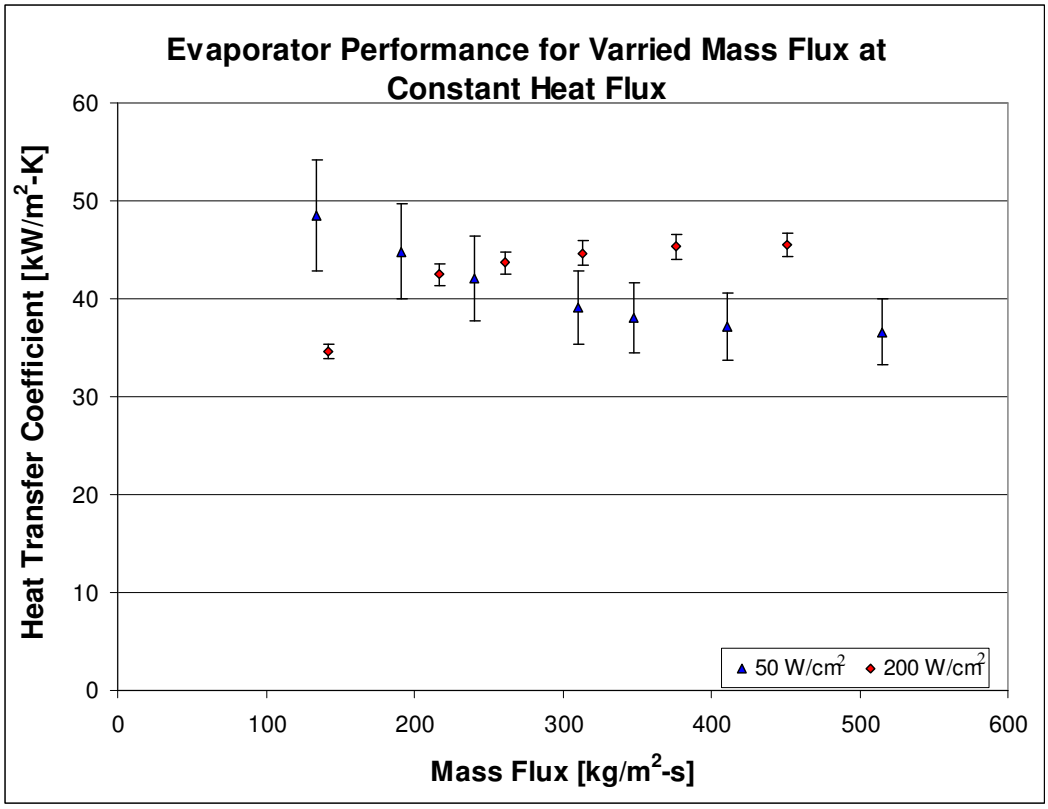

Figure 36: Evaporator Results at Constant Heat Flux

In the tests where heat flux was changed, mass fluxes of 263 and 485 kg/m^2-s were selected. These represent the middle and maximum values available with this test setup and are comparable to the mass fluxes for most of the first-generation tests. As mentioned in Chapter 3, the mass flux for these tests was not kept exactly constant due to changes in system pressure drop caused by density changes and the change in quality at the evaporator exit. At 485 kg/m^2-s, the actual mass flux varied up to 7 percent with lower variation at 263 kg/m^2-s. The results of these tests are shown in Figure 37 and Figure 38. Like the tests above, these show almost no difference in performance between the two mass fluxes. Similarly, heat flux has little effect on performance above about 800 kW/m^2.

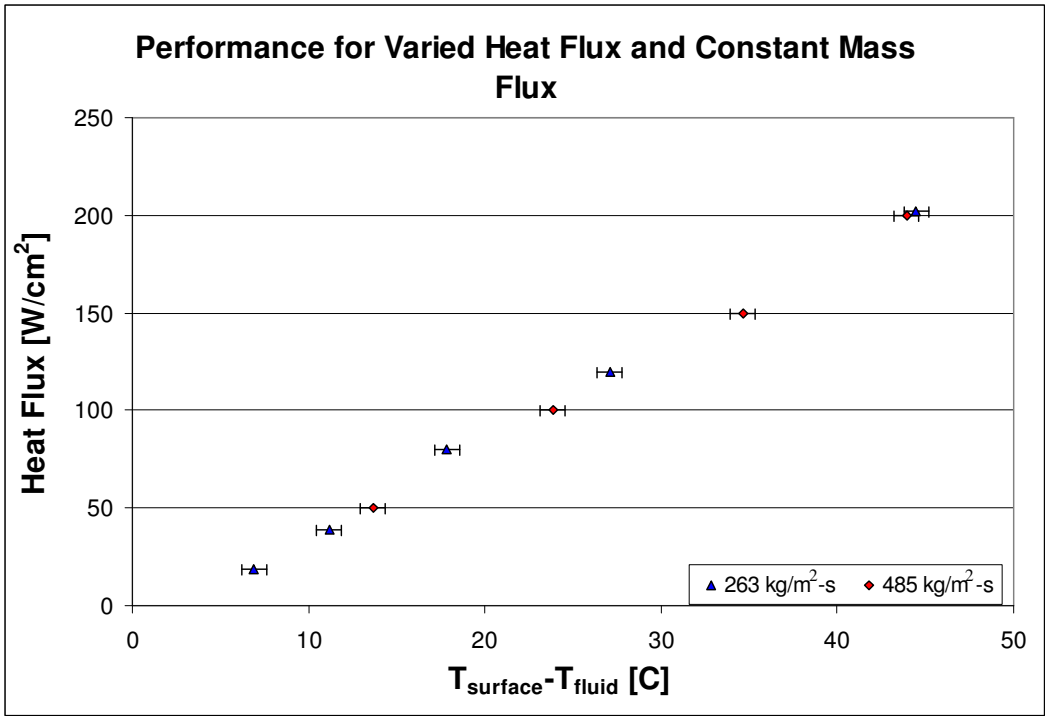

Figure 37: Evaporator Results at Constant Mass Flux

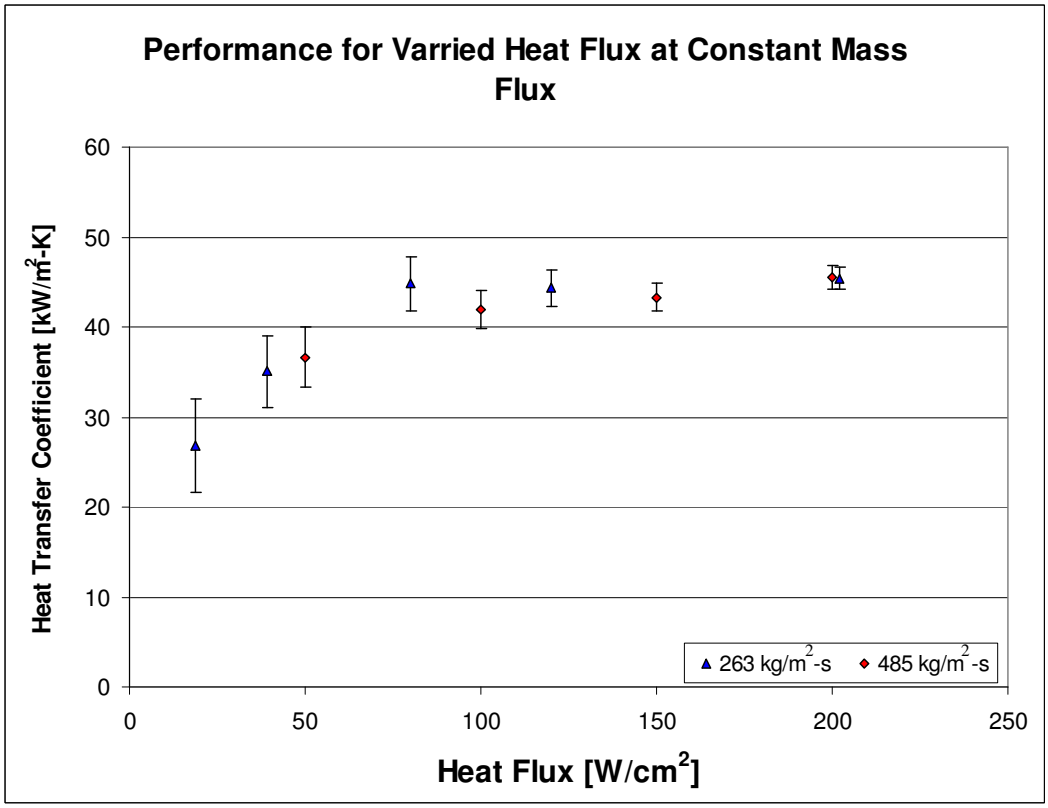

Figure 38: Evaporator Results at Constant Mass Flux

Figure 39 shows the pressure drop performance for the constant heat flux test that was conducted. As one would expect, the pressure drop increases linearly with increased mass flux. Additionally, the higher heat flux test shows higher pressure drop due to the increased two-phase pressure drop component. The magnitude of the pressure drop was not expected however. Based on preliminary findings with the first generation test setup, and the conceptual design of the force-fed evaporation process, a smaller pressure drop was expected. It is not known why the pressure drop would be so high based on the physical configuration of the setup and the mass flux applied.

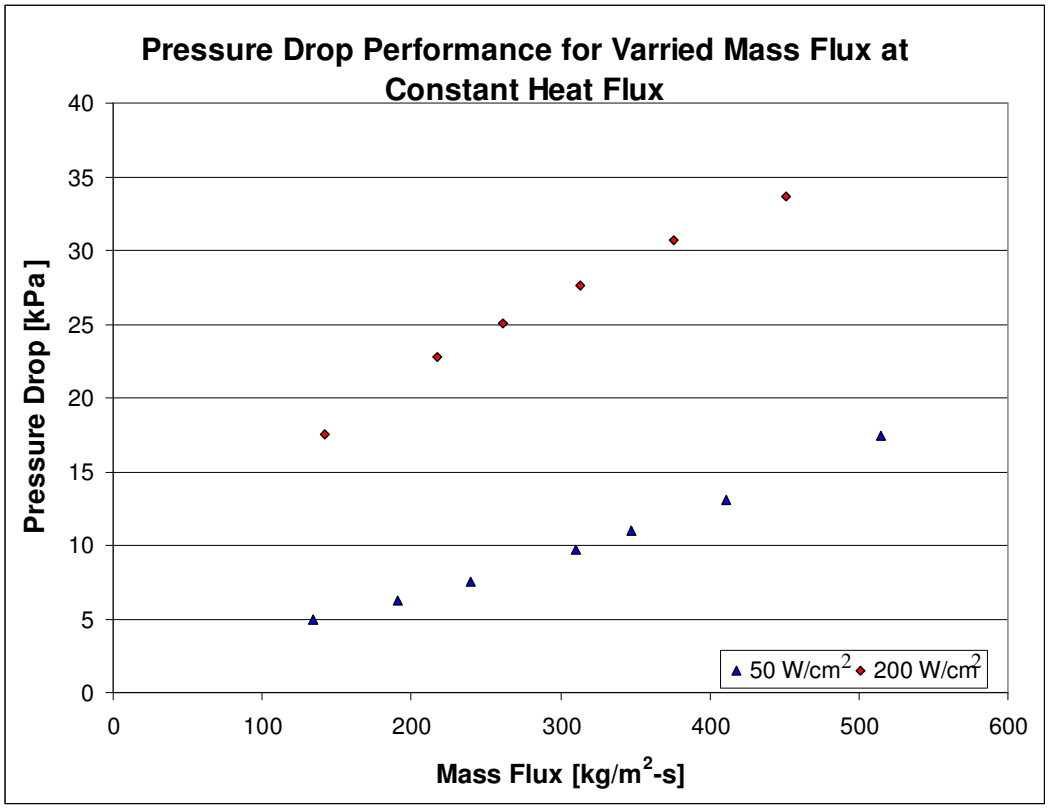

Figure 39: Pressure Drop Results at Constant Heat Flux

There are a few possible explanations for why mass flux has such a small effect in these tests compared with the first-generation tests. In the first-generation tests, the major effect of increased mass flux was seen when the mass flux of HFE-7100 was increased by a factor of 6.3 from 362 to 2,297 kg/m^2-s, while the present tests cover an increase of only a factor of 1.8. So it may be that these tests simply do not span a large enough range in mass flux for a noticeable effect to be seen. It is also possible that mass flux only plays an important role above some value. The other possible reason is that the difference in the test section design may cause mass flux to play an important role in the first-generation tests and not the second. This design difference is explored below.

Another noticeable difference between the first and second-generation results is the thermal performance of the evaporators. The second-generation test section and test setup were designed with the expectation of attaining even higher heat transfer coefficients and heat fluxes. As it turns out, the heat transfer coefficients are notably lower than the previous tests, and consequently the maximum heat flux also does not outperform those tests. It is believed that the reason for this is due to the difference in the header design between generations 1 and 2 and generations 3 and 4. In the former, fluid is supplied in a manner that may cause it to jet into the evaporator surface with an effect similar to jet impingement, but with lower velocities than true jet impingement. Additionally, the small diameter of the inlet tube—seen as a disadvantage from a pressure drop standpoint—increases the inlet velocity, which would enhance this effect. In the later

generations, fluid is supplied parallel to the surface through larger flow passages. According to the theory for force-fed evaporation discussed in Chapter 3, both designs are equivalent, because both header types provide alternating channels for inlet and exhaust; however because the actual flow phenomena are very complicated, particularly for two-phase flow, it may be that these two types of headers create very different effects. A possible flow pattern for the second generation header is explored in the conclusions in Chapter 7. This difference sheds additional light on the result noted above—that mass flux is only seen to impact evaporator performance in the first-generation test setup. Mass flux is known to affect thermal performance in impingement flows, and an impingment-like flow pattern may be a contributor to the performance of the first-generation header designs.

The results presented in this chapter confirm one of the initial expectations for this project, which formed one part of the motivation or it. They show that force-fed technology, applied to evaporators, can produce very high heat transfer coefficients and very high heat flux. As various evaporator configurations were tested, more was learned about how the force-fed process works. Some of this knowledge was incorporated into the system-level design, and all of it can be used as the starting point for future research in this field. The next chapter discusses the results of the system-level tests.

Chapter 6: System-Level Results and Discussions

5.1: First-Generation Cold Plate

The experimental setup and procedures for these tests were described in Chapter 4. The goal of these tests was to test the concept of the self-contained, two-phase cold plate and to provide information for the construction of a more developed plate. Additionally, the tests were intended to investigate component performance while pushing the cold plate to its maximum system capacity.

A great deal was learned from the experiments conducted with this first-generation cold plate. During the initial tests, numerous problems with the piezoelectric diaphragm pump were encountered. In addition to the lower-than-desired flow rate, which was expected based on earlier pump testing, the pump repeatedly cracked its diaphragm while running. This necessitated the diaphragm being replaced each time, and in general prevented useful testing of the cold plate with this pump. As a result, the micro-gear pump mentioned in Chapter 4 was used to test the system.

A second issue became apparent during early testing which needed to be resolved. Even with the condensers cooling the fluid to 10℃ or more below the saturation temperature, some non-equilibrium vapor bubbles remained in the liquid line heading to the pump. Allowing these bubbles to flow through the pump prevented it from operating effectively. Additionally, because these vapor

bubbles were unable to flow through the evaporator microchannels, they caused a build-up of vapor in the liquid line feeding the evaporators, causing dryout. To remedy this, the tubes running to the gear pump were rearranged so that the fluid passed from the cold plate to a reservoir and then to the pump and back into the plate. Doing this ensured that the fluid had sufficient time for mixing to occur in the reservoir, which eliminated the bubble problem. As mentioned in Chapter 4, this modification also made the plate less "self-contained;" however, it was deemed necessary for testing this first-generation system.

With these changes made, thermodynamic testing of the cold plate was carried out very successfully. The heat transfer coefficient of each evaporator and condenser was calculated from the data obtained during the test. For the evaporators, the area used to calculate this is the area of the heater—1 cm^2—rather than the area of the surface—1.96 cm^2—because for the plate's target application, it is the area of the electronics chip which is important. For the condensers, the surface and the cooler have the same area—7 cm^2—so this value was used. The heat transfer coefficient for the evaporators was calculated using the fluid temperature as the average of the incoming liquid temperature and the exiting two-phase mixture temperature. Similarly, the calculation for the condensers used the average of two-phase and liquid temperatures.

The results for the first tests, conducted with HFE-7100, are shown below in Figure 40, Figure 41, and Figure 42. Figure 40 shows Evaporator 1 with the best

performance, followed by Evaporator 4. During testing, Evaporators 3 and 4 actually tended to perform the best. Evaporator 1 was run at a lower power than Evaporator 4 which affected their relative performances. This was required because Evaporators 1 and 2 tended to overheat before 3 and 4. This is believed to be caused by uneven flow distribution so that Evaporators 3 and 4, closest to the pump, received the highest flow rates, while Evaporators 1 and 2, around the corner, received less flow. In general, the evaporators did not perform as well in the cold plate as they did in the single evaporator tests discussed in Chapter 5. At full plate power, the evaporator heat transfer coefficients ranged from 42 to 56 kW/m^2-K, compared with a maximum of 90 kW/m^2-K for a single evaporator test with comparable mass flux. A major reason for the lower thermal performance is the degree of subcooling that was necessary to prevent vapor bubbles forming in the liquid supply to the evaporators. In addition, the mass flux in the cold plate was at most 243 kg/m^2-s in the evaporators. The exact system flow rate was not recorded because the plate does not include a flow meter, but it was believed to be significantly below the pump's maximum output, which means the mass flux was somewhat less here than in the individual evaporator tests with HFE-7100.

For the two condensers, the heat transfer coefficient at maximum power was 19 kW/m^2-K, which is also less than could be achieved in a single condenser test. The maximum mass flux—based on pump maximum output—would be 125 kg/m^2-s, which is a high estimate as before. This performance is also believed to be caused by the subcooling. When condensing the working fluid, a great deal of

heat is transferred with a relatively small change in temperature. When subcooling the fluid, a relatively small amount of additional heat is transferred with a large change in temperature. This causes the heat transfer coefficient—a measurement of heat dissipated per degree—to be reduced. As one would expect, there exists a positive, and roughly linear, relationship between plate power and condenser heat transfer coefficient. This is because higher plate power means that higher quality fluid leaves the evaporators and enters the condensers. This higher quality fluid permits more heat to be transferred during that small change in temperature. It is interesting to note that both condensers exhibited nearly equal performance. Although they were arranged in series, so that Condenser 2 supplied most or all of the subcooling, the method of calculating the heat transfer coefficient causes the two condensers to exhibit comparable performance.

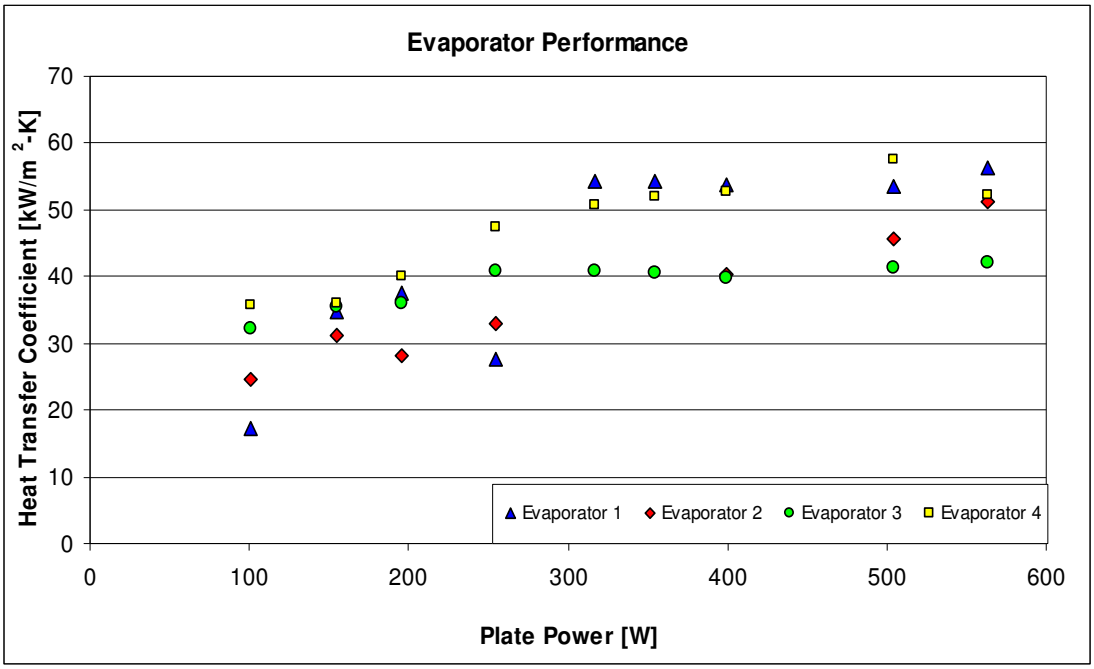

Figure 40: First-Generation Cold Plate Evaporator Performance using HFE-7100

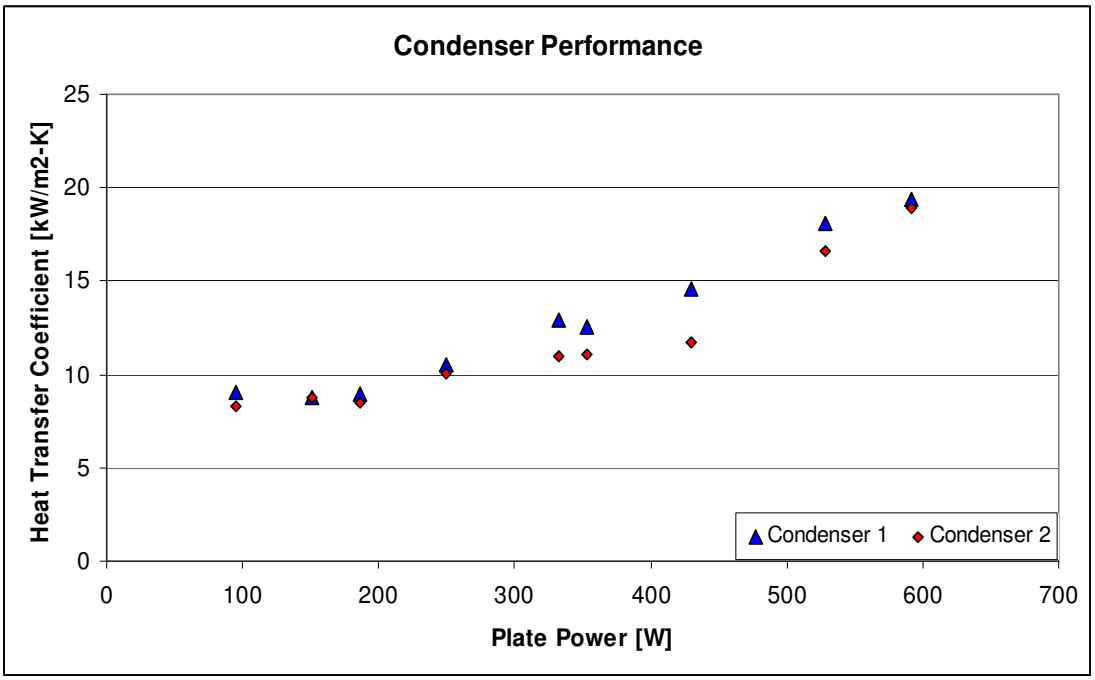

Figure 41: First-Generation Cold Plate Condenser Performance using HFE-7100

Figure 42 shows the pressure drop for various plate locations. The first item that is apparent from the graph is that the results are highly scattered. This is a result of the fact that the system parameters are in constant fluctuation. Part of the cause for this is that bubble formation in the evaporators is erratic, which causes pressure drop to be erratic. The small volume of this system amplifies this effect and ensures that it will be seen throughout the plate. One can see that evaporator pressure drops are generally below 2 kPa, and condenser pressure drops—which are measured across both condensers due to their series arrangement on the plate—were generally below 1.5 kPa. These values are relatively low for such a high heat flux system, which is in keeping with the expectations for the design of these force-fed components.

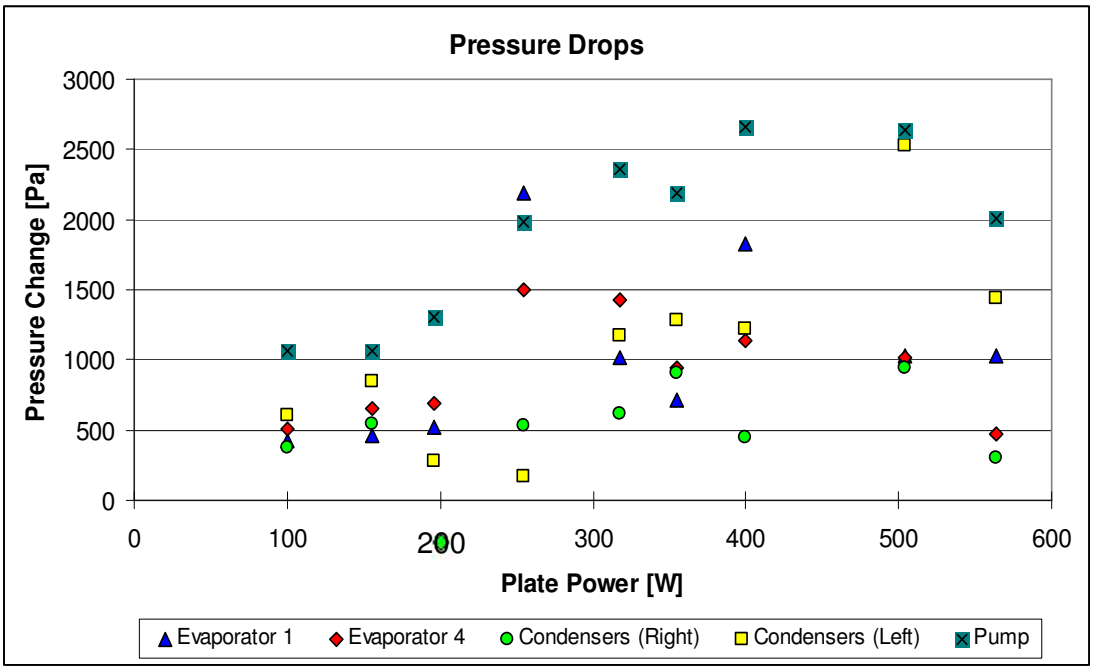

Figure 42: First-Generation Cold Plate System Pressure Drops

Following the tests conducted with HFE-7100, brief tests were conducted with a mixture of methanol and water. This fluid was chosen for a number of reasons. Methanol and water both have much better thermal properties than HFE-7100. Though water is the better of the two, methanol is added to counteract water's high boiling point. 30% methanol in this mixture is the limit to be considered non-flammable, which was the reason for selecting this ratio. The results of these tests—two data points at 695 and 1030 W—are shown in Figure 43 and Figure 44 along with the HFE-7100 data presented above.

It is immediately apparent from the graphs below that the methanol-water mixture allowed the plate to reach a much higher capacity, nearly double what was attained with HFE-7100. It is believed that this improved performance is due largely or entirely to the new fluid's thermal characteristics. Figure 43 shows that

the heat transfer coefficient for Evaporator 4 improved considerably with the new fluid and reached a level of 157 kW/m^2-K, which is nearly as high as the value reached in Chapter 5 with a single evaporator and a much higher mass flux of HFE-7100. However, the other evaporators showed only modest improvements in heat transfer coefficient, which shows that flow distribution continued to be problematic in these tests.

The condensers, shown in Figure 44, displayed performance that matched the previously noted semi-linear relationship. Both condensers displayed similar performance; however, Condenser 2 pulled ahead with slightly better performance, for a maximum heat transfer coefficient of 36 kW/m^2-K.

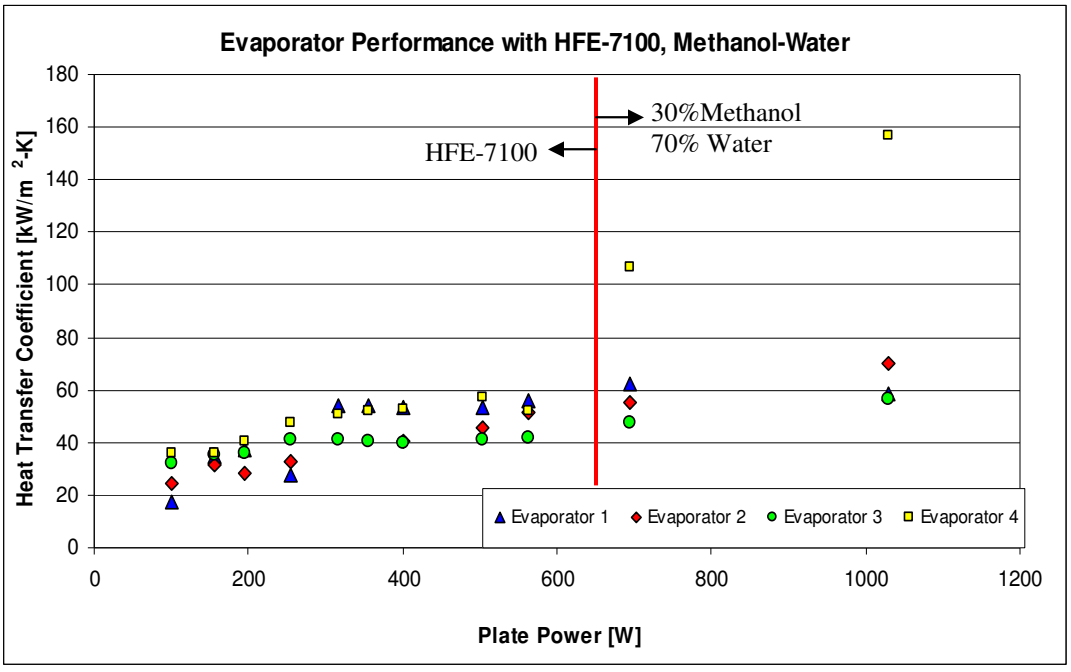

Figure 43: First-Generation Cold Plate Evaporator Performance with Methanol-Water

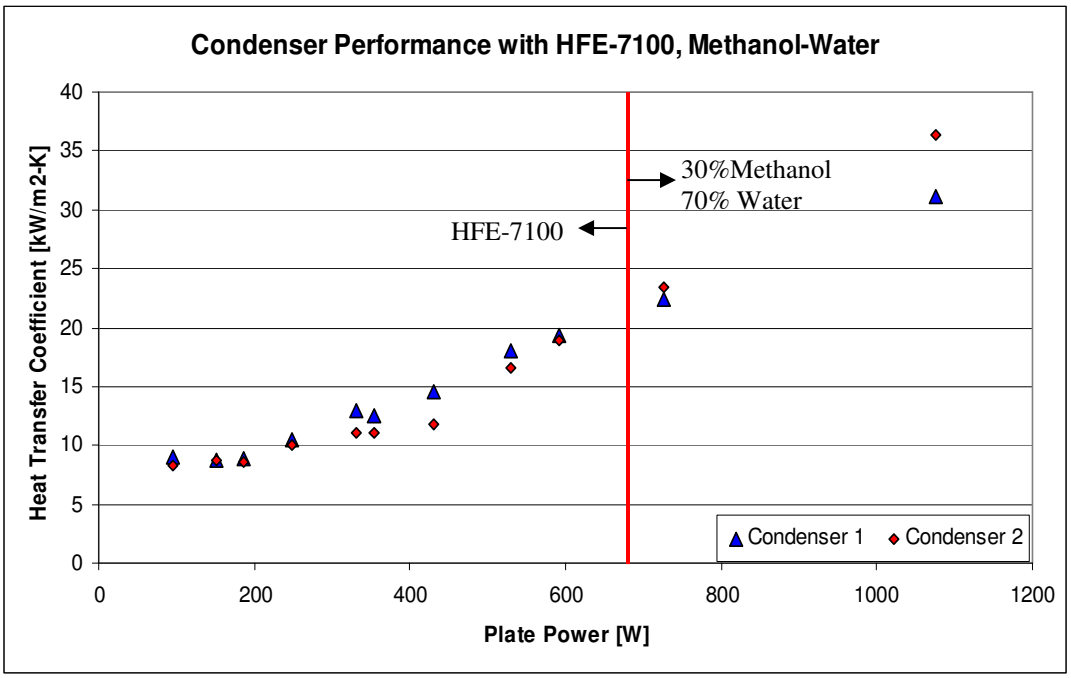

Figure 44: First-Generation Cold Plate Condenser Performance with Methanol-Water

As mentioned above, poor flow distribution was identified as the primary hindrance to higher plate capacity and better component performance. The evaporators and condensers never reached their performance limits based on prior component testing. Because the pressure drop through the force-fed structures was low—on the order of 500 to 1500 Pa—the liquid working fluid being fed to the evaporators preferred to pass through the first two evaporators, rather than turning the corner to adequately feed the second two. More importantly, some vapor bubbles from the first two evaporators would escape toward the liquid side and be carried to the second two evaporators. This caused vapor build-up at those two evaporators, which deprived them of liquid flow. This vapor build up contributed to the instabilities in the temperature and pressure measurements, and made data collection difficult at high powers. It also caused the second two evaporators in particular to overheat at lower powers then they would otherwise

be capable of reaching. The 10°C of subcooling used to counteract this permitted testing to the level attained, but such a degree of subcooling could not be maintained by the water chiller for higher powers.

Another problem that was noted during testing was leakage past the evaporators and condensers. It was not possible to quantify this leakage; however, it is believed to be a relatively small portion of the total flow. Leakage occurred between the component header and the Delrin wall forming the side of the flow channel and between the header and the bead of silicone used to seal the areas between evaporators. This leakage probably played a small part of the lower-than-expected thermal performance of the components. Knowledge of these possible leakage flow paths guided the development of the second-generation cold plate component modules as well as the overall design of the plate.

Based on the information gained from these tests, improved flow distribution was identified as a major input for the design of the second-generation cold plate described in Chapter 4. The need to exclude vapor bubbles from the pump and the evaporator supply line was also carried to the second-generation design. Incorporating these improvements into the second-generation design led to notably better performance in these areas.

6.2: Second-Generation Cold Plate

The redesigned cold plate that grew out of the improvements above produced many of the desired results. The use of a common rail with a set of valves to supply fluid to the evaporators improved flow distribution. The possibility of bubbles being carried downstream from one evaporator to another was eliminated entirely due to the separation between the supply rail and the evaporator itself. Likewise, the flow paths to each of the evaporators were balanced to create more evenly distributed flow. The evaporators closer to the top of the plate have a longer flow path; however, the pressure drop in the header should be much less than the pressure drop in the evaporator, which would mitigate the effect of this difference in path length. The valves can be used to completely nullify the effect of the header pressure drop, and this action is planned for later testing, which is outside the scope of this work.

The reservoir incorporated into the second-generation cold plate was successful in removing vapor bubbles from the liquid stream sent to the pump. 7 - 9°C of subcooling of the fluid leaving the condensers was still present because this was not designed as a controllable parameter. Leakage around the components was not possible due to the modular design of the system; there is no flowpath which bypasses the evaporators or condensers except leakage out of the system, of which no appreciable amount was detected. There is, however, reason to believe that leakage within the components was a problem; this will be discussed below. All the tests on this system were performed with R-245fa.

Figure 45 shows the thermal performance of the evaporators against the total power absorbed and dissipated by the plate. The maximum capacity the plate reached was 1.92 kW, significantly more than the capacity of the first-generation cold plate. This limit was imposed by the test setup, which was unable to supply any more power to the evaporators; the system itself did not exhibit any indication that it was approaching its capacity limit. The thermal performance of the evaporators shows that the heater temperatures were still within reason, so it is believed that the plate can reach still higher powers. As with the first-generation cold plate, the heat transfer coefficient is specified relative to the size of the heaters. The fluid temperature used is the saturation temperature of the fluid, which causes some error at low heat flux but is acceptable at higher heat fluxes. At the maximum plate power, the heat transfer coefficients ranged from 50 to96 kW/m^2-K. These values are somewhat better than what was achieved in the first-generation cold plate. There is an apparent decrease in performance at increasing power, which may be due to the method of calculating the heat transfer coefficient. With this level of thermal performance, the effect of dissipating 1.92 kW—1,600 kW/m^2 average on the heaters—is a 17-32°C temperature rise from the heater to the fluid. This is within the range which should be acceptable for electronics cooling, and better flow distribution could result in more balanced temperature rises across all of the devices.

The performance of the condensers, shown in Figure 46, was similar to the first-generation cold plate. The devices had similar heat transfer coefficients which increased roughly linearly with power and reached a maximum value of 23 kW/m^2-K. The explanation given for the first-generation cold plate that heat transfer coefficient increases with increasing vapor quality applies here as well. The major difference between these condensers and those in the first-generation cold plate is their size, and consequently their heat flux. The available area for condensation increased by a factor of 6.6 compared with 4.4 for the evaporators and a factor of 4 for the area of the plate itself. In the original cold plate, the heat was removed from the condensers by soldered-in-place copper slots with high turbulence and pressure drop. Such an arrangement would not be possible for cooling most applications, so the second-generation plate was cooled with the plate-and-tube heat exchanger discussed in Chapter 4. This setup creates a much higher thermal resistance from the cooling water to the working fluid, so a larger area is necessary to reject heat with a reasonable temperature rise. This large area creates lower mass flux in the condensers, which is a likely cause for their relatively low performance.

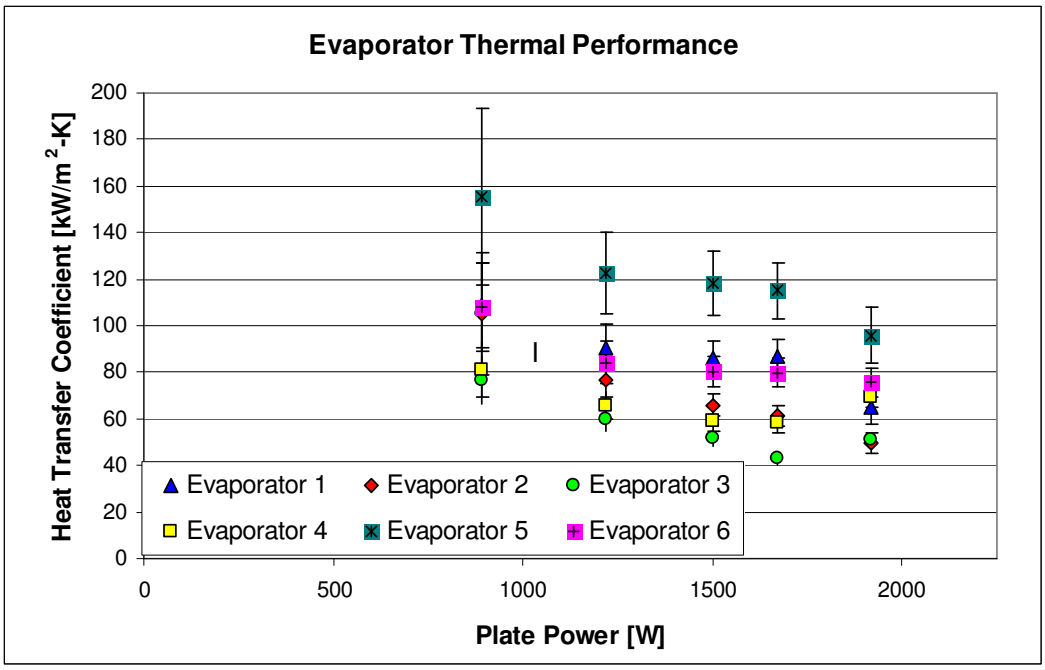

Figure 45: Second-Generation Cold Plate Evaporator Performance

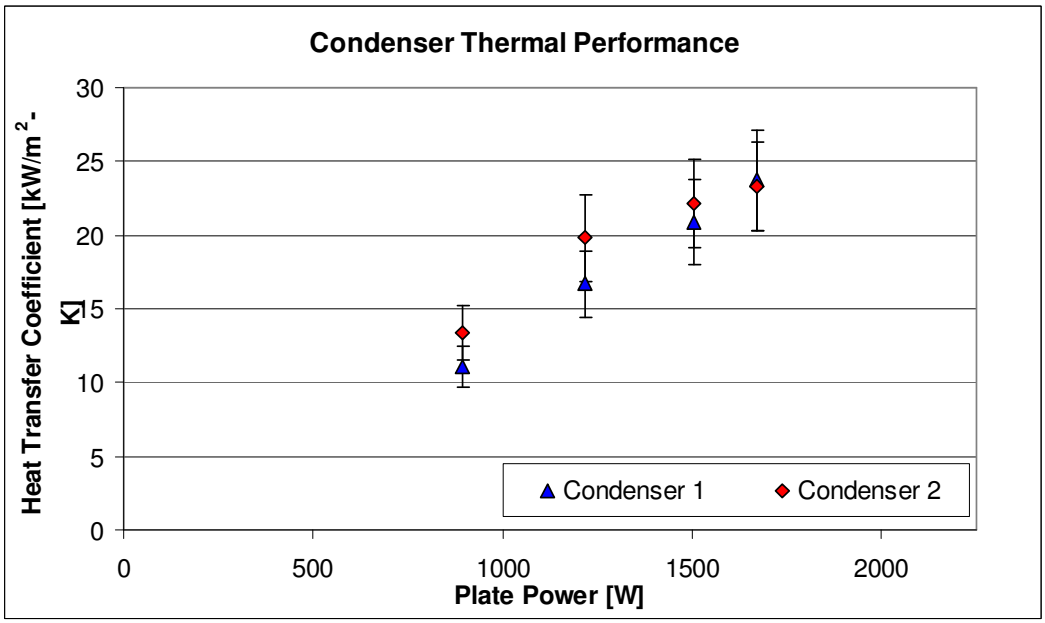

Figure 46: Second-Generation Cold Plate Condenser Performance

The pressure drop performance of the cold plate components is shown in Figure 47 and Figure 48. Compared with the first-generation cold plate, these evaporators show much more orderly pressure drops. As power increases,

pressure drop increases roughly linearly due to the increased vapor formation which adds to pressure drop. However, at 4 to 8 kPa, the pressure drops were much higher in the second-generation plate. The condensers showed a slight decrease in pressure drop with increasing power, but the pressure drops were much higher at 10-25 kPa. This was not expected because the larger area available for condensation should have reduced the pressure drop. However, the pressure measurement locations are at the inlet and outlet tubes from the components, which is an area of high velocity. This high velocity contributes to the measured pressure drop even though it is not pressure drop across the actual heat exchanger. The high velocity at the outlet also causes the measured pressure drop across the evaporator to erroneously include a portion of the dynamic pressure according to Bernoulli's equation. The flow rate in this cold plate could not be determined because the system pressure drop is close to the pump's maximum, which makes the pump curve not usable. A rough estimate of mass flux based on the published pump curve is up to 221 kg/m^2-s in the evaporators and 72.57 kg/m^2-s in the condensers.

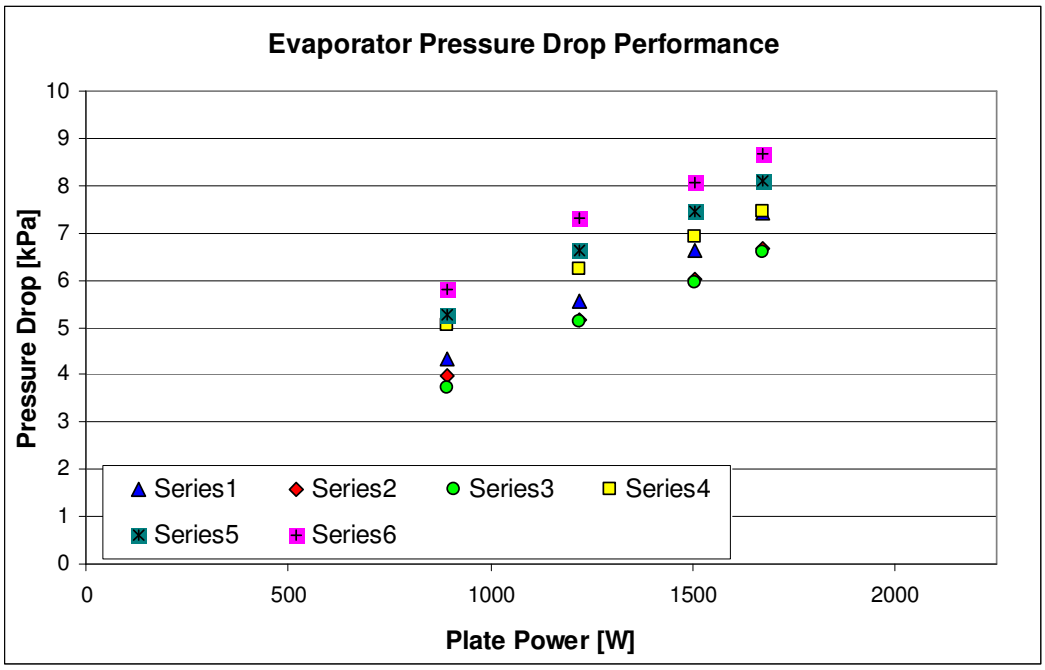

Figure 47: Second-Generation Cold Plate Evaporator Pressure Drop

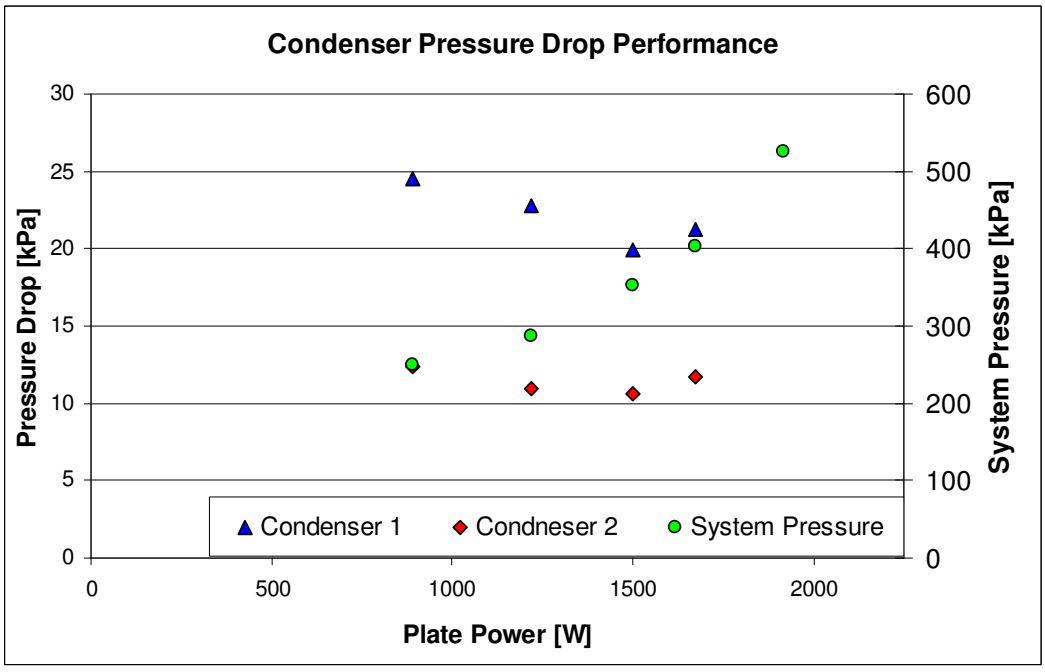

Figure 48: Second-Generation Cold Plate Condenser Pressure Drop

As mentioned previously, the cold plate functions as a heat spreader as it absorbs heat in the compact evaporators and dissipate it to the large plate-and-tube heat

exchanger. The ratio of condenser size to heater size causes the heat transfer area to be increased by a factor of 8.66. The temperature difference from the microchannel surface to saturation temperature was relatively constant for the condensers, while at the evaporators, it increased with increasing heat flux. This caused the ratio of evaporator ΔT to condenser ΔT to range from about 0.9 to 2.6 throughout the tests. This shows the value of the heat spreading nature of the plate: at higher powers, the larger condenser area is able to maintain a lower saturation temperature, which leads to a lower heater temperature.

Although the evaporators and condensers in the second-generation cold plate performed well enough to absorb and reject almost 2 kW with reasonable system parameters, they did not perform as well as was expected based on results of component testing and the improvements made with the fourth-generation style headers. It is believed that this performance gap is the result of defects in the components caused by the hand fabrication process. The processes used to make the modules are mass-production processes—stamping, folding, vacuum bonding—but the manual processes by which they were executed allowed room for errors that would be worked out in advance of a mass production operation. In particular, it is the bonding process which seems most likely to have affected the plate's performance. If the top and bottom of the "C" shape failed to bond to the module casing and the microchannel surface, fluid could leak by without entering the microchannels, which would degrade performance. This does not explain the

high pressure drops, but it is also possible that the bonding process might have damaged the fine surface of the device and reduced available flow area.

As mentioned in Chapter 4, the first-generation cold plate was the first attempt to run a small-scale system using the force-fed process. As such, the positive results of the tests on this system are very remarkable, while the shortcomings of the test setup are not surprising. The second-generation test setup eliminated many of these shortcomings and was able to achieve significantly better results. Even with these advancements discovered and implemented, there remains a wealth of knowledge waiting to be uncovered about the force-fed evaporation and condensation processes. A great deal can still be learned from the test setup used in this research, and still more could be discovered from small-scale fundamental experiments and even larger scale system studies. This work simply scratches the surfaces by demonstrating the ability of the force-fed process to generate very high heat transfer coefficients and operate in a self-contained system to dissipate a large amount of heat from a high-power electronics system.

Chapter 7: Conclusions and Future Work

7.1: Conclusions

This work presents the results of research into the performance of the force-fed evaporation process and its applicability to cooling of high flux electronics on a large-scale basis, including cooling of large circuit boards or other heat exchanger applications. The project objectives—to investigate the thermal performance of force-fed evaporators and to develop a self-contained, two-phase cold plate—have both been accomplished. The component-level tests have demonstrated that force-fed evaporators can dissipate extremely large heat fluxes at high heat transfer coefficients. These high heat transfer coefficients automatically suggest that these devices may be ideal for cooling high-power circuits of high-power electronics. The low pressure drop observed during testing furthers this conclusion, as low pressure drop corresponds to low required pumping power for the cooling system.

The second half of this project, which showed the successful development of a functioning two-phase cooling loop, confirms that force-fed technology is particularly well suited to electronics cooling. The developed cold plate was capable of dissipating a large heat load while maintaining reasonable temperatures on the heaters. Equally important, the device was able to contain all of the necessary components in a small device which is capable of being packaged together with the circuit board which it cools. These accomplishments—

supported by additional research in this area—put force-fed technology on the forefront of emerging cooling technologies and close to the point of market introduction.

During component-level testing, the force-fed evaporators dissipated close to 10,000 kW/m^2 and obtained heat fluxes as high as 160 kW/m^2-K with HFE-7100 and significantly higher with ethanol. These levels vastly exceeded the initial expectations for the force-fed process when this project was initiated. The most noteworthy conclusion from the details of these tests is the degree to which header configuration affects the performance of the force-fed process. The second generation header aimed the flow directly at the surface—possibly creating an effect like a low-velocity relative of jet impingement—while the design of the third and fourth generation headers would not have created any such effect. This explains many of the differences in the results between the first and second-generation test setups. Heat transfer coefficients were generally better across the board in the tests which incorporated this more directed flow pattern.

Additionally, with the impingement-like effect, a large increase in flow rate produced a very large improvement in heat transfer coefficient and maximum heat flux. In the second-generation setup, which lacked such an impingement-like effect, there was no strong correlation between mass flux and heat transfer coefficient. There was also not a significant correlation between heat flux and heat transfer coefficient in the experiments with the second-generation test setup.

Figure 49 below is a diagram similar to the one in Figure 5. It shows what is believed to be the actual flow pattern in the second generation header which produced the impingement-like effect. It shows how the primary liquid flow path is straight down into the evaporator surface. The last important conclusion drawn from the component-level tests is the fact that the data shown in Figure 34 closely resembled the shape of a standard pool-boiling curve. This emphasizes the relationship between the force-fed process and flow boiling, which also exhibits a boiling curve similar to the pool boiling curve.

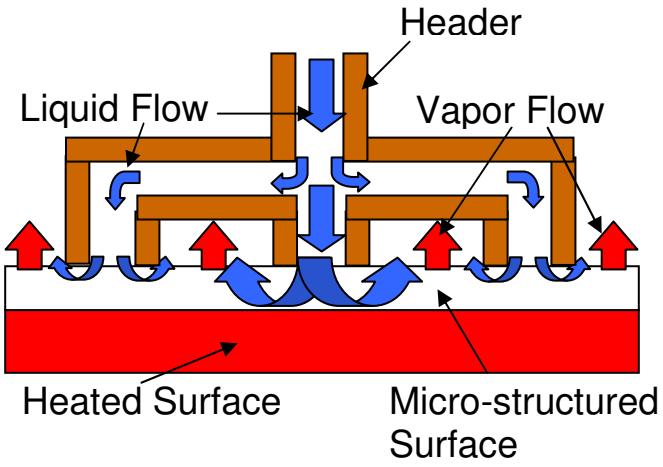

Figure 49: Force-Fed Flow Pattern in Second Generation Header

The system-level tests demonstrated that stability is a significant concern for a low-volume, two-phase test setup. The natural fluctuations in pressure and flow rate which occur for all two-phase systems—as described in Chapter 2—are amplified in a small system which causes flow pulsation and reversal to dominate the system behavior. This issue can be mitigated with significant subcooling and the use of a sufficiently large reservoir for phase separation, which work together to ensure that only liquid is sent to the pump and evaporators. The other principal

concern for small, two-phase systems is flow distribution. Space limitations make it difficult to build ideal tubing configurations between components; however, the flowpaths to each of the components must be balanced to develop good performance. Good flow distribution also helps counteract system instability by ensuring an even flow of liquid to the evaporators.

The other system-level findings, which are not surprising, include the observation that leakage can present a major challenge when developing a system that packages such complicated devices into so small a space. Also, it was noted that the performance of the individual components was somewhat lower in the complete system compared with individual tests due to less-than-ideal conditions before and after a given component. Despite this, the cold plate was able to deliver a cooling capacity of 1.92 kW with evaporators operating at 50-96 kW/m^2-K with 1,600 kW/m^2 average dissipated at the heaters. This was obtained with a pressure drop no higher than about 8.5 kPa, which shows that the force-fed evaporation process is able to deliver high performance at an acceptable pressure drop in a compact package.

The conclusions and results which have come out of this research make an important addition to the understanding of the force-fed process and to the understanding of small, self-contained, two-phase cooling systems. This technology offers a great deal of promise for the future of computer cooling, and

it is hoped that other research will continue to deepen the understanding of it so that it can be brought to a commercial market.

7.2: Recommendations for Future Work

The experiments conducted as a part of this work have only begun to uncover all that can be learned about the force-fed evaporation and condensation processes. Compared with more established cooling methods, force-fed technology is in its academic infancy. At present, there are at least four different directions in which future research could head. At the component-level, there is opportunity to develop a force-fed evaporator that incorporates an impingement-like effect in a package which is suitable for incorporation in a larger, self-contained system. This would bring to fruition a cold plate with a modular and widely applicable design and with the extremely high thermal performance shown by evaporators in the present research. Additionally, work can be done to optimize the design of the surface and header channels to squeeze even more performance out of the evaporators.

At the sub-component level, research can be done to understand the fundamental mechanics of the force-fed process. In the present work, even the component-level tests which used a 1 cm^2 sample still included close to 800 of the smallest functional "cells" of the force-fed process: a single microchannel with a single inlet and exhaust. This fundamental understanding would allow this technology

to be confidently applied to a wider variety of applications and would aid in finding the optimum evaporator design discussed above.

At the system level, many more tests need to be done to understand how the self-contained, two-phase system operates under a wider variety of circumstances. This is the research which is most necessary for bringing this technology to market: a fully functioning plate cannot be designed and used until one understands how it will function under all operating conditions. In particular, testing is needed in the areas of system performance with unequal power distributions, system performance with quickly fluctuating power levels, and system performance in a non-horizontal orientation. Research can also focus on developing larger and more intricate cold plates to determine how the system will respond to this added complexity.

Finally, research is needed which focuses on the application of force-fed technology to the condensation process. Force-fed condensation is utilized in the system-level tests in the present research, but no detailed study was conducted for this project. All of the research discussed for force-fed evaporators should also be conducted for condensation. Force-fed condensers are vital to developing a self-contained, force-fed system with a small footprint. Improving the performance of the condensers will impact system performance about as much as improving evaporator performance.

It is clear that opportunities abound for further research in this field. The force-fed process described in this project is an exciting new field with immediate relevance to electronics cooling and a variety of other applications. While it is believed that the present work makes a valuable contribution to the development of this technology, there is no doubt that future research is necessary for this new technology to get off the ground and become a viable option for advanced electronics cooling. When this occurs, it is believed that the force-fed process will become an indispensable part of the future of electronics cooling.

Bibliography

[1] McCluskey, F. P. "Lecture for ENME 780." 2007. University of Maryland, College Park.

[2] Wilson, J., Guenin, B. "Cooling solutions in the past decade." Electronics Cooling Online. 2005. http://www.electronics-cooling.com/html/2005_nov_article1.html. Last visited on November 5, 2007.

[3] "Why the need for liquid cooling." Thermacore Thermal Management Systems. http://www.thermacore.com/lcs_need.htm. Last visited on May 18, 2006.

[4] Kim, J. "Lecture for ENME 647." 2006. University of Maryland, College Park.

[5] Tuckerman, D. B. & Pease, R. F. W. "High-performance heat sinking for VLSI." IEEE Electronic Device Letters. 2 (1981) 126–129.

[6] Kandlikar, S. G. "Heat Transfer Mechanisms During Flow Boiling in Microchannels." ASME Journal of Heat Transfer. 126 (2004) 8–16.

[7] Boye, H., Staate, Y., Schmidt, J. "Experimental investigation and modeling of heat transfer during convective boiling in a minichannel." International Journal of Heat and Mass Transfer. 50 (2007) 208-215.

[8] Pamitran, A. S., Choi, K.-I., Oh, J.-T., Oh, H.-K. "Forced convective boiling heat transfer of R410A in horizontal minichannels." International Journal of Refrigeration. 30 (2007) 155-165.

[9] Bao, Z. Y., Fletcher, D. F., Haynes, B. S. "Flow boiling heat transfer of Freon R11 and HCFC123 in narrow passages." International Journal of Heat and Mass Transfer. 43 (2000) 3347-3358.

[10] Diaz, M. C. & Schmidt, J. "Experimental investigation of transient boiling heat transfer in microchannels." International Journal of Heat and Fluid Flow. 28 (2007) 95-102.

[11] Jiang, L., Wong, M., Zohar, Y. "Forced convective boiling in a microchannel heat sink." Journal of Microelectromechanical Systems. 10 (2001) 80-87.

[12] Chen, T., & Garimella, S. V. "Flow boiling heat transfer to a dielectric coolant in a microchannel heat sink." IEEE Transactions on Components and Packaging Technologies. 30 (2007) 24-31.

[13] Yun, R., Heo, J. H., Kim, Y. "Evaporative heat transfer and pressure drop of R410A in microchannels." International Journal of Refrigeration. 29 (2006) 92-100.

[14] Chang, K. H. & Pan, C. "Two-phase flow instability for boiling in a microchannel heat sink." International Journal of Heat and Mass Transfer. 50 (2007) 2078-2088.

[15] Kandlikar, S. G. & Balasubramanian, P. "An experimental study on the effect of gravitational orientation on flow boiling of water in 1054 x 197 μm parallel minichannels." Journal of Heat Transfer. 127 (2005) 820-829.

[16] Chen, C.-H. "Forced convection heat transfer in microchannel heat sinks." International Journal of Heat and Mass Transfer. 50 (2007) 2182-2189.
[17] Zhao, C. Y. & Lu, T. J. "Analysis of microchannel heat sinks for electronics cooling." International Journal of Heat and Mass Transfer. 45 (2002) 4857-4869.
[18] Kandlikar, S. G. "Two-phase flow patterns, pressure drop, and heat transfer during boiling in minichannel flow passages of compact evaporators." Heat Transfer Engineering. 23 (2002) 5-23.
[19] Thome, J. R. "Boiling in microchannels: a review of experiment and theory." International Journal of Heat and Fluid Flow. 25 (2004) 128-139.
[20] Thome, J. R. "State-of-the-art overview of boiling and two-phase flows in microchannels." Heat Transfer Engineering. 27 (2006) 4-19.
[21] Zhuang, C. F., Ma, C. F., Qin, M. "Experimental study on local heat transfer with liquid impingement flow in two-dimensional micro-channels." International Journal of Heat and Mass Transfer. 40 (1997) 4055-4059.
[22] Jang, S. P., Kim, S. J., Paik, K. W. "Experimental investigation of thermal characteristics for a microchannel heat sink subject to an impinging jet, using a micro-thermal sensor array." Sensors and Actuators. 105 (2003) 211-224.
[23] Jang, S. P. & Kim, S. J. "Fluid flow and thermal characteristics of a microchannel heat sink subject to an impinging air jet." Journal of Heat Transfer. 127 (2005) 770-779.
[24] Lee, D.-Y. & Vafai, K. "Comparative analysis of jet impingement and microchannel cooling for high heat flux applications." International Journal of Heat and Mass Transfer. 42 (1999) 1555-1568.
[25] Copeland, D., Behnia, M., Nakayama, W. "Manifold microchannel heat sinks: isothermal analysis." IEEE Transactions on Components, Packaging, and Manufacturing Technology. 20 (1997) 96-102.
[26] Pak, B. C., Chun, W. C., Baek, B. J., Copeland, D. "Forced air cooling by using manifold microchannel heat sinks." Advanced Electronic Packaging. 2 (1997) 1837-1842.
[27] Sung, M. K. & Mudawar, I. "Correlation of critical heat flux in hybrid jet impingement/micro-channel cooling scheme." International Journal of Heat and Mass Transfer. 49 (2006) 2663-2672.
[28] Baummer, T. B., Al-Hajri, E., Ohadi, M. M., Dessiatoun, S. V. "Forced convection boiling in microchannels for improved heat transfer." Proceedings of the ASME Fourth International Conference on Nanochannels, Microchannels, and Minichannels. 2006.
[29] Baummer, T., Cetegen, E., Ohadi, M., Dessiatoun, S. "Force-fed evaporation and condensation utilizing advanced micro-structured surfaces and micro-channels." Thermal Challenges in Next Generation Electronics Systems. 2007.
[30] "Standard Products: Cold Plates." Lytron. 2006. http://www.lytron.com/standard/cold_plates.asp. Last visited on October 25, 2007.